Characteristics and Trends of the Campbell Plateau Meander in the Southern Ocean: 1993-2020

Xinlong Liu[1,2*], Amelie Meyer[1,2], and Christopher C. Chapman[3]

[1]Institute for Marine and Antarctic Studies, University of Tasmania, Battery Point, TAS, Australia.
[2]Australian Research Council Centre of Excellence for Climate Extremes, University of Tasmania, Battery Point, TAS, Australia.
[3]CSIRO (Commonwealth Scientific and Industrial Research Organisation) Environment, Climate, Atmosphere Oceans Interaction Program, Battery Point, TAS, Australia.

Key Points:

- The position of the Campbell Plateau meander has remained stable for the past 30 years, apart from a section downstream shifting northward.
- The amplitude of the Campbell Plateau meander has been decreasing (flatter) upstream of the Plateau and increasing (steeper) downstream.
- The Campbell Plateau meander has been widening and accelerating over the 1993-2020 period, especially downstream of the Plateau.

*Current address: Institute for Marine and Antarctic Studies, 20 Castray Esplanade, Battery Point, TAS, Australia 7004

Corresponding author: Xinlong Liu, xinlong.liu@utas.edu.au

Abstract

Meanders are significant features of the Antarctic Circumpolar Current in the Southern Ocean and sites of enhanced upwelling, cross-frontal tracer fluxes, and exchanges between the surface and deep ocean. They often overlap the locations of fronts and are linked to topographic features. While much is known about Southern Ocean fronts and how they are changing, the response of meanders to climate change is largely unexplored. In this study, we investigate the Campbell Plateau meander south of New Zealand. We apply a local gradient maxima method to satellite altimetry data to identify the position of the meander and estimate its width, geostrophic current speed, and associated trends from 1993 to 2020. We find that the position of the meander has been relatively fixed, except for a section downstream of the Plateau, which has shifted northward by about 0.4° latitude per decade. The meander has become flatter at the western edge of the Plateau, but steeper at the eastern edge of the Plateau. Overall, the meander has widened by 2 km per decade and accelerated by 0.01 $m\ s^{-1}$ per decade, particularly downstream of the Plateau. These findings are consistent with other work on standing meanders in the Southern Ocean. Increases in eddy kinetic energy and of the South Pacific Gyre index support our hypotheses that changes in the downstream jet stability and the South Pacific Gyre contribute to these observed trends. The impacts of these trends on cross-frontal transport remain to be evaluated.

Plain Language Summary

In the Southern Ocean, meanders are parts of the Antarctic Circumpolar Current that deviate from the usual west-to-east flow by having a substantial north-south component, resulting in a wave-like appearance. Standing meanders are meanders that are stationary and do not move much over months and years. They are a special feature of the Antarctic Circumpolar Current and are fundamental for exchanges between the surface and deep ocean. Although changes in the Antarctic Circumpolar Current have been well studied, especially in the context of climate change, very little is known about how Southern Ocean meanders are changing. This study focuses on the Campbell Plateau meander south of New Zealand in the Southern Ocean. Using ocean sea surface height data from satellites, we analyse the monthly position of this meander, estimate its monthly width and speed, and quantify how these characteristics have changed over the 1993-2020 period. Upstream of the Campbell Plateau, the meander has undergone almost no changes in its position, width or speed. However, downstream of the Plateau, the meander has shifted northward, widened and accelerated. These trends are consistent with other observations in the Southern Ocean, and we discuss potential mechanisms to explain them.

1 Introduction

The Southern Ocean is crucial in the context of global climate by being a major sink of anthropogenic heat and carbon dioxide (Rintoul & Naveira Garabato, 2013; Frölicher et al., 2015; Bindoff et al., 2019) through the upwelling of deep waters and their subsequent downwelling, which produces a large proportion of global deep waters (Toggweiler & Samuels, 1995; Lumpkin & Speer, 2007; J. Marshall & Speer, 2012; Morrison et al., 2015). The Southern Ocean has absorbed about 40% of global oceanic carbon dioxide over the past two centuries (Sabine et al., 2004; Mikaloff Fletcher et al., 2006; Sallée et al., 2012). Its predominant circulation feature is the deep-reaching Antarctic Circumpolar Current (ACC), which manifests as the southward shoaling of tilted isopycnals (Rintoul & Naveira Garabato, 2013) and carries approximately 170 Sv (Sverdrup; 1 $Sv = 10^6\ m^3\ s^{-1}$) of water eastward (Donohue et al., 2016). Primarily driven by the strong mid-latitude westerly winds and buoyancy forcing, the ACC links the Atlantic, Indian, and Pacific Oceans, conveying climate signals by transporting heat, momentum, and other tracers

(Sabine et al., 2004; Sarmiento et al., 2004; Olbers et al., 2004; Sallée et al., 2012; Rintoul & Naveira Garabato, 2013).

The Southern Ocean is also known for its abundance of eddies, which are related to the instabilities of the ACC and have significant impacts on Southern Ocean dynamics and thermodynamics (Y. Zhang et al., 2021). The Southern Ocean is characterised by some of the highest global eddy kinetic energy values (EKE; Fu et al. (2010)) and receives over 60% of the total wind energy input to the global ocean (Hughes & Wilson, 2008). EKE measures the energy associated with time-varying currents. EKE usually increases downstream of significant topography features (Gille et al., 2000) such as the Kerguelen and Campbell Plateaus (Y. Zhang et al., 2021), as stored available potential energy within the tilted isopycnals is released (Thompson & Naveira Garabato, 2014). EKE downstream of the Campbell Plateau has strong increasing decadal trends (Y. Zhang et al., 2021).

In the Southern Ocean, the transition from warmer subtropical waters to colder Antarctic waters as one travels south does not occur smoothly but is instead concentrated into a series of sharp transition zones (Deacon, 1937), called 'fronts', which are generally aligned east-west (Deacon, 1937; Chapman et al., 2020; Thomas et al., 2021). Fronts delimit the borders of separate water masses that each have unique environmental characteristics (Orsi et al., 1995) and tend to correspond to sites of narrow, high-velocity currents known as 'jets' (Sokolov & Rintoul, 2002, 2007b). These fronts suppress the meridional exchange of heat and tracers in the Southern Ocean (Naveira Garabato et al., 2011; Thompson & Sallée, 2012; Chapman & Sallée, 2017).

In some regions of the Southern Ocean, these fronts have a non-zonal orientation (Hughes, 2005; Sokolov & Rintoul, 2007a). Such 'meanders' are generated by the interactions between the ACC and large topographic features (Thompson, 2010; Thompson & Sallée, 2012; Dove et al., 2021, 2022) such as the Campbell Plateau and the Kerguelen Plateau (e.g., Roach et al. (2016); Klocker (2018)). Standing meanders are meanders that have little to no temporal variability over timescales of weeks to months: they follow the same path over time. Several standing meanders such as the Campbell Plateau standing meander and the Agulhas-Kerguelen standing meander (e.g., Meyer et al. (2023)) are found along the ACC. These standing meander regions are recognised as dynamical hotspots, where upwelling (Viglione & Thompson, 2016; Tamsitt et al., 2017; Brady et al., 2021), subduction (Llort et al., 2018; Bachman et al., 2017; Dove et al., 2021), cross-frontal exchanges (Langlais et al., 2011; Thompson & Sallée, 2012), vertical momentum transport (Thompson & Naveira Garabato, 2014), and eddy energy (Gille & Kelly, 1996; Witter & Chelton, 1998; Lu & Speer, 2010; Chapman et al., 2015; Rosso et al., 2015; Foppert et al., 2017) are enhanced. Standing meanders can greatly impact horizontal current transport with strong meridional deviations from the zonal flow of up to 5° latitude (Nardelli, 2013; Phillips & Bindoff, 2014; Thompson & Naveira Garabato, 2014). Thompson and Naveira Garabato (2014) also show that the meanders 'flex' under wind forcing, and this response propagates vertically through the water column. Compared with quieter downstream regions, Southern Ocean standing meanders regions stand out with larger lateral buoyancy gradients and increased variability in the mixed layer depth, and show signs of stronger ocean mixing (Thompson & Naveira Garabato, 2014; Langlais et al., 2017).

While studies have assessed the response of the ACC fronts to climate change, less work has focused on meanders and their trends. A majority of meander studies have looked at dynamic mechanisms, energy transport, and their role in the Southern Ocean system (e.g., Thompson and Sallée (2012); Chapman et al. (2015); Barthel et al. (2017); Youngs et al. (2017); Barthel et al. (2022); Meijer et al. (2022); X. Zhang et al. (2023); Cyriac et al. (2023)). Although a few studies such as Thompson and Naveira Garabato (2014) and Meyer et al. (2023) have investigated long-term changes and trends of meanders, further research is needed to fully understand the trends of meanders over time. By using

a global ocean model with a realistic eddy field, Thompson and Naveira Garabato (2014) report the response of meanders to increased wind forcing, which includes steeper isopycnals, increased curvature, and changing wavelength and amplitude of the meanders. An observational study of the Agulhas-Kerguelen standing meander in the southwest Indian Ocean has also identified trends in the curvature of the meander, its width and speed over the past 30 years (Meyer et al., 2023).

Considering the importance of Southern Ocean meanders, it is key that we better understand how they are changing and what the impacts of these changes might be on the climate system. In this study, we apply a "local" front detection method to satellite altimetry data to identify and characterise the trends of the Campbell Plateau meander in the Southern Ocean over the 1993-2020 period. The Campbell Plateau, mostly shallower than 1000 m depth, is located in the southwestern Pacific sector of the Southern Ocean (Neil et al., 2004; Forcén-Vázquez et al., 2021). It extends about 1100 km southeast of South Island, New Zealand. The Plateau largely constrains the eastward flow of the ACC (Gordon, 1972; Orsi et al., 1995), which leads to a significant northward deviation of the ACC along its eastern boundary (Heath, 1981; Carter & Wilkin, 1999; Morris et al., 2001). We find that overall, the Campbell Plateau meander has been relatively spatially stable except for its downstream section which has moved northward. The meander has been significantly widening and accelerating over the 1993-2020 period. In this paper, we propose two, non-mutually exclusive hypotheses to explain these observed trends of the meander: 1. Changes in the jet stability downstream of the Campbell Plateau, especially the spatial and temporal patterns and trends of EKE downstream of the Plateau; and 2. changes in the large-scale South Pacific Gyre circulation. We assess some evidence for each of these hypotheses. The remaining sections of this manuscript are organised as follows. Section 2 describes the data for investigating the characteristics and trends of the meander and the meander analysis methods. Section 3 presents the characteristics and identified trends of the meander. In Section 4, we discuss the possible mechanisms for explaining the observed trends of the meander, which include jet stability, gyre strength and their implications. Finally, we summarise the key findings of this study in Section 5.

2 Data and Methods

2.1 Satellite Altimetry Data

In this study, we use the AVISO absolute dynamic topography and surface geostrophic current speeds products from multi-mission satellite altimetry (CMEMS, 2023) spanning over the 1993-2020 period to identify and characterise the Campbell Plateau meander. The AVISO sea level anomaly products are also used to investigate changes in the South Pacific Gyre between 1993 and 2020 (AVISO, 2023).

2.2 Gridded Data

We also use the *in-situ* temperature data from the Roemmich-Gilson gridded Argo product (Argo, 2023). This product provides temperature fields from the surface to 2000 m depth on a regular $1^\circ \times 1^\circ$ latitude and longitude grid, spanning the period 2006-2022. This product is used to investigate changes in the thermal structures of the Campbell Plateau meander.

2.3 Atmosphertic Reanalysis Data

In addition, we use the surface zonal and meridional surface (10 m) wind speeds from the JRA-55 (Japanese 55-year Reanalysis) atmospheric products over the 1993-2020 period to analyse the temporal trends of zonal and meridional wind speeds over the Camp-

bell Plateau region (Onogi et al., 2007). Only data for the period corresponding to the satellite altimetry product are used here, to have trends over a comparable time period.

2.4 Meander Position Identification

The meander position identification methodology used in this study belongs to the broader family of "local gradient maxima" methods (Chapman, 2017; Chapman et al., 2020). Chapman (2017) applied this methodology to fronts in the Southern Ocean. The method was then modified by Meyer et al. (2023) for the Agulhas-Kerguelen standing meander and further adjusted in this study for the Campbell Plateau meander. Generally speaking, there are two kinds of definitions for Southern Ocean fronts and thus meanders: local definitions and global definitions (Chapman et al., 2020). Local definitions use properties found in the local vicinity of a geographical position to evaluate if a front exists (Chapman et al., 2020). The 'gradient thresholding' method, which we apply here, is perhaps used most frequently. It identifies the presence a front or meander when the gradient of a quantity (e.g., sea surface temperature (SST): Moore et al. (1999); Dong et al. (2006); Freeman et al. (2016) or sea surface height (SSH): Hughes and Ash (2001); Chapman (2014, 2017)) is larger than a predetermined threshold value.

We choose to apply the local gradient method on sea surface height because the alternative global method based on sea surface height contours is impacted on decadal time scales by the large-scale steric height tendency that is linked to the warming of the Southern Ocean (Gille, 2014). As pointed out by Sokolov and Rintoul (2009), in long-term position trends of sea surface height contours, it is challenging to identify what part of the trend is driven by frontal displacement and what part is driven by increasing sea level (Gille, 2014). Fronts and meanders identified by global methods are also more indicative of spurious temporal variability (Graham et al., 2012; Gille, 2014) and the choice of the number of fronts is fixed, which makes it difficult to identify changes in the structure of fronts and meanders (Graham et al., 2012; Chapman, 2017). Although some studies have explored changes in frontal position using satellite SST data (e.g., Moore et al. (1997, 1999); Dong et al. (2006)), in this study, we choose absolute dynamic topography because it captures both surface and subsurface ocean processes (Lapeyre, 2009), while SST is representative of ocean surface conditions only. Since the ACC can be assumed equivalent barotropic (Killworth, 1992) particularly when averaged over several eddy time cycles (Phillips & Bindoff, 2014), we assume that the surface signature of the meander is broadly reflective of the current at depth.

We apply three main steps to identify the position of the Campbell Plateau meander:

1. Derive the **gradients** of absolute dynamic topography in the Campbell Plateau region (30°S-70°S and 150°E-210°E; shown in Figure 1 (a) and (b)).
2. Identify the **daily position** of the meander. This is defined as areas where the absolute dynamic topography gradient exceeds a relative threshold. This definition is applied to every daily snapshot of the absolute dynamic topography gradient maps over the 1993-2020 period. Selecting the appropriate relative threshold value requires finding a balance between identifying enough meander signals without including too many non-meander features such as eddies. We choose 25% of the maximum absolute dynamic topography gradient as the relative threshold based on sensitivity tests (see Figure B.1 in Appendix B.1 of X. Liu (2022) for details).
3. Obtain the **time-averaged positions** of the meander. By summing the total number of times that the meander is identified at each point in the Campbell Plateau region over a certain period of time, we derive the meander frequency (similar to the frontal frequency in Chapman (2017)), which we can use to produce the meander's monthly occurrence maps over a period of several months. We choose a

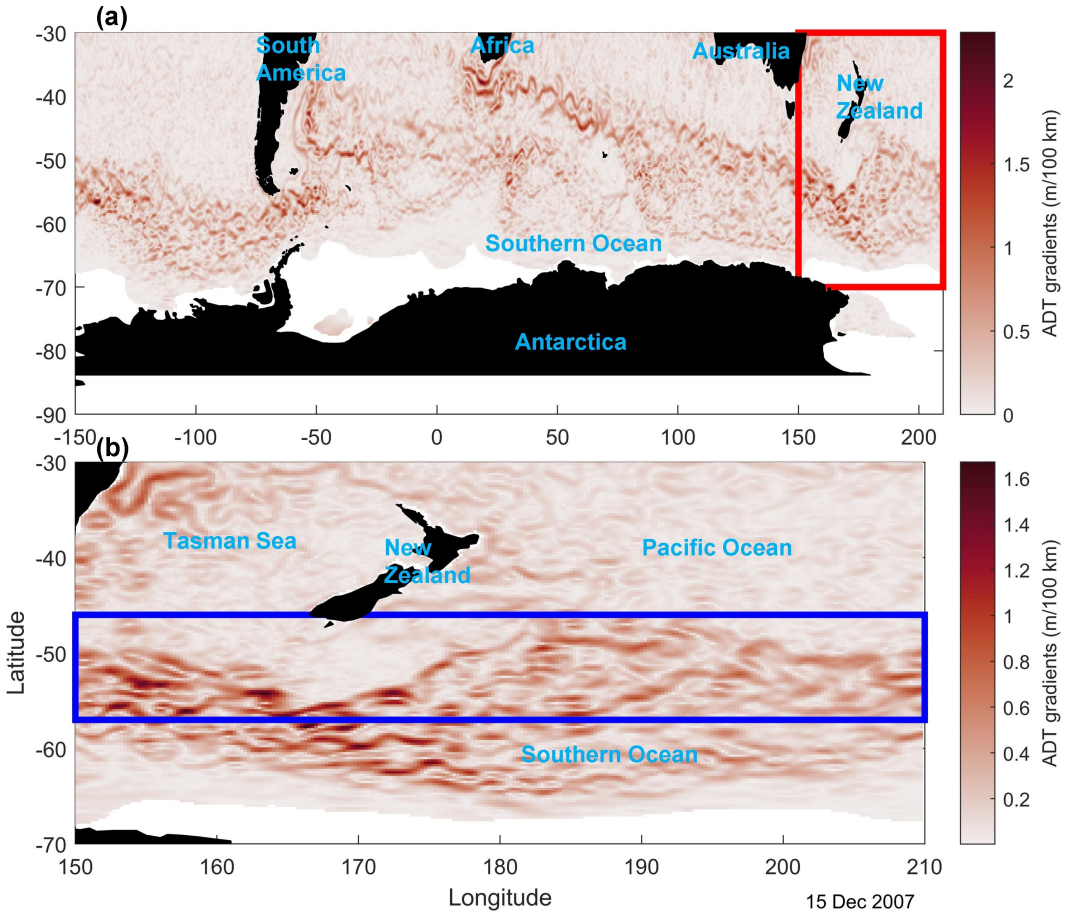

Figure 1. Snapshot of absolute dynamic topography (ADT) gradients in m/100 km on 15 December 2007 in (a) the Southern Ocean and (b) the Campbell Plateau region. The red rectangle in (a) represents the Campbell Plateau region shown in (b), which is the study region. The blue rectangle in (b) indicates the smaller domain where the meander's latitude and longitude positions are identified. White areas are regions where no satellite altimetry data were available.

4-month period to estimate occurrence as this smooths out the shorter time-scale variability including eddies, and retains the longer-term signals that are of interest (see Figure B.2 in Appendix B.2 of X. Liu (2022) for details).

The final product is the monthly longitude and latitude position of the meander. We zoom into a subsection of our domain (46°S-57°S and 150°E-210°E; Figure 1 (b), blue rectangle), which is the smallest area where we can identify the meander continuously in the Campbell Plateau region, to ignore frontal signals outside the marked meander area. Next, we determine the peak meander frequency at each latitude and longitude in this smaller domain, which identifies the position of the meander (Figure 2 (b) and (c) red star). Note that the monthly meander position sometimes has 'jumps' and 'spikes' (Figure 2 (a), blue line). These 'jumps' are usually due to eddies freshly detached from the meander that have a strong gradient in absolute dynamic topography (see Figure B.3 in Appendix B.3 of X. Liu (2022) for an example).

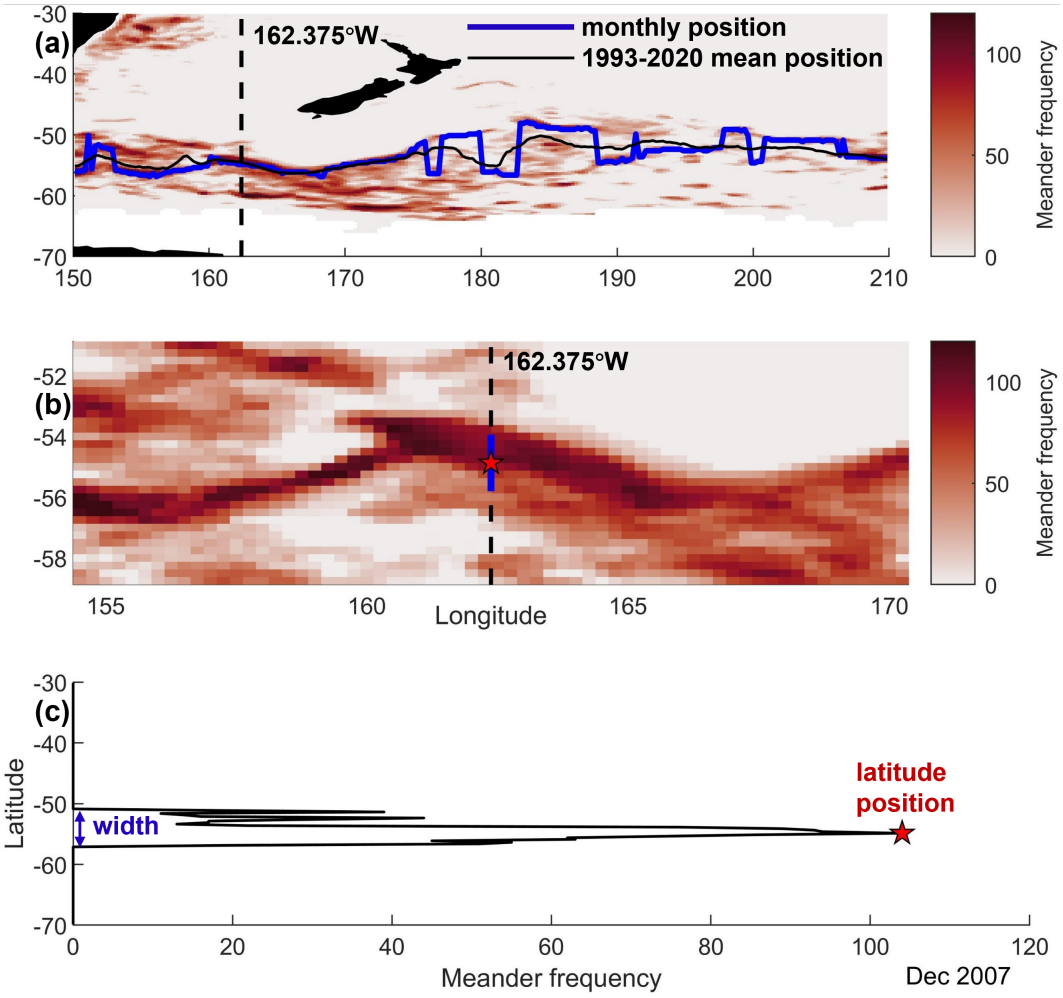

Figure 2. (a) Meander's monthly position (thick blue line) for December 2007 and 1993-2020 meander mean position (thin black line) over the meander frequency occurrence for the 4-month sum period; (b) Meander's width range (vertical solid blue line) together with its latitude position (red star) at 162.375°E over the meander frequency occurrence for the 4-month sum period; (c) Meander frequency transect at 162.375°E with meander latitude position (red star) and width range (blue arrow). White areas in (a) are regions where no satellite altimetry data were available.

Table 1. Longitude ranges of the peaks, troughs, and sections of the Campbell Plateau meander used in this study.

	Longitude Ranges
Meander Peaks	
Peak 1	156.6°E-157.1°E
Peak 2	159.1°E-159.6°E
Peak 3	164.9°E-165.9°E
Peak 4	180.2°E-181.4°E
Meander Troughs	
Trough 1	157.9°E-158.6°E
Trough 2	159.9°E-160.9°E
Trough 3	177.1°E-177.6°E
Trough 4	183.9°E-184.9°E
Meander Sections	
Upstream Section	150.0°E-158.4°E
Plateau Section	158.4°E-184.4°E
Downstream Section	184.4°E-210°E
Flat Region	191.6°E-204.9°E

2.5 Meander Characteristics

We estimate the width of the meander based on the meander frequency: for each longitude, the width of the meander is taken to be the sum of the meridional distances between the latitude of the meander frequency peak and the latitude where the frequency is zero to the north and south (northern and southern boundaries) (Figure 2, blue line in (b) and blue arrow in (c)). We also identify the monthly position of four key standing peaks and four troughs of the meander and estimate the monthly amplitude in two regions (Table 1; Figure 3). We define the peaks as the southernmost points (farthest from the equator) and troughs as the northernmost (closest to the equator) points of the meander's trajectory (Newton, 1959; Meijer et al., 2022) for each month, within the manually-defined longitude ranges (Table 1). These peaks and troughs are consistently identifiable over the 1993-2020 period and are labelled Pk 1 to Pk 4 and Tr 1 to Tr 4 from west to east (Figure 3). The amplitude of the meander at two sets of peaks and troughs is then estimated as half of the meridional distance (in degrees latitude) between these adjacent peaks and troughs. While identifying the positions of the peaks and troughs is automated, quality control involves manual checks. We also derive the monthly geostrophic current speed over the 4-month sum period using the daily zonal and meridional geostrophic velocities.

2.6 Statistical Trends

To investigate trends in the position, width and geostrophic current speed of the meander over the 1993-2020 period, we apply a linear regression to the monthly time series. Then, a time-lagged analysis using multiple linear regression ($\hat{y} = b_0 + b_1 x_1 +$

$b_2x_2 + ... + b_kx_k$) is applied to all the derived trends to test for statistical significance. Each of the k predictor variables has a coefficient corresponding to the slope in the linear regression. The intercept (or regression constant) is expressed as b_0. These $k + 1$ coefficients are often recognised as the regression parameters. We also test for autocorrelations in the time series and the associated autocorrelation time scales. In this study, we choose a 3-month lag as it removes part of the seasonal and sub-seasonal variability in the time series that we are not investigating and is adequately short to avoid the potential autocorrelation time scales of the dataset. The sample autocorrelation functions of the monthly trends and their 95% confidence intervals are also estimated using the test of residual analysis with autocorrelation. Detailed figures for these autocorrelation tests are in Appendix A of X. Liu (2022).

3 Results

3.1 Meander Trajectory

When investigating the trajectory of the meander, we identify four areas in the Campbell Plateau region where the meander dynamics are distinct: an 'Upstream Section' west of the Campbell Plateau, a 'Plateau Section' south of the Plateau, a 'Downstream Section' east of the Plateau, and a 'Flat Region' farther downstream of the Plateau where the shape of the meander is flatter than in other sections (Figure 3; details in Table 1).

The ACC enters the study domain from the west at approximately 55°S (Figure 3, Upstream Section). It encounters and is modified by the Macquarie Ridge (Figure 3, Trs 1 and 2; Pks 1 and 2). When the ACC encounters the Macquarie Ridge, its long-term mean position flows through a shallower canyon (2000 m depth; about 52.0°S) rather than the deeper canyon (4000 m depth; about 53.3°S; Figure 3, Upstream Section). Next, the meander continues to flow eastward and is steered by the Campbell Plateau and the Subantarctic Slope, flowing along a boundary between 4000 m and 6000 m depth (Figure 3, Plateau Section). Eventually, the current flows into the Downstream Section, where the interaction between the meander and topography is weaker than upstream, with almost no topographic impact except near the far eastern boundary (Figure 3, Downstream Section). The trajectory in the Downstream Section is relatively zonal (less flexed) with fewer wave features, especially in the highlighted 'Flat Region' (Figure 3, Flat Region). The locations of the peaks and troughs are related to regional topography with several peaks and troughs linked to local ridges, seamounts and other topographic features (Figure 3).

3.2 Observed Changes in Meander Position

We investigate the temporal trends of the meridional displacement, width, and geostrophic current speed of the Campbell Plateau meander to identify long-term changes (if any) in this meander system. We estimate these trends based on both the full-resolution monthly time series and a smoothed rolling-mean time series. The trends for the meridional displacement, width and geostrophic current speed of this meander are very similar whether estimated with the monthly time series or with the rolling-mean data (not shown) and here, we present the monthly data results.

We find that the mean position of the whole meander has been significantly moving northward by 0.12° latitude per decade latitude per decade from 1993 to 2020 (Figure 4 (a); Table 2). This overall trend hides regional variations in displacement (Figure 4 (a); Table 2). Apart from some small-scale variability, the Upstream and Plateau sections of the meander are relatively stationary between 1993 and 2020 with small non-significant trends (0.04° and -0.02° latitude per decade, respectively; Figure 3 and 4 (a), Upstream and Plateau sections). In contrast, the Downstream Section has a significant northward moving trend of 0.30° latitude per decade (p=0.000, R^2=0.324; Figure 4 (a),

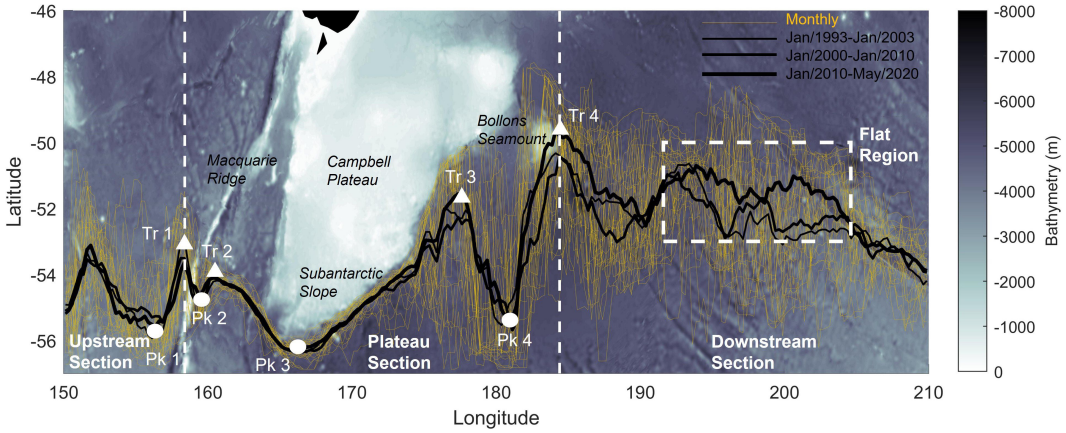

Figure 3. The Campbell Plateau meander's mean positions over three different decades (black lines) and monthly positions at the ten-month interval (yellow lines) between 1993 and 2020. Four peaks (white circles) and four troughs (white triangles) of the meander are marked along the meander's trajectory (Pk 1 to Pk 4 and Tr 1 to Tr 4). Also indicated are the Flat Region (white dashed rectangle) and the three sections (Upstream, Plateau, and Downstream) of the meander.

Table 2. Linear decadal trends and their associated statistics for the Campbell Plateau meander's meridional displacement (position) in degree latitude per decade ($^\circ$ *lat/dec*), width in kilometre per decade (*km/dec*), and geostrophic current speed (speed) in $m\ s^{-1}$ per decade ($m\ s^{-1}/dec$) based on the monthly data time series over the 1993-2020 period. Statistically significant trends are indicated with *.

	Position ($^\circ$ lat/dec)	*Width (km/dec)*	*Speed ($m\ s^{-1}$/dec)*
Whole Meander	+0.12* (p=0.000, R^2=0.264)	+2.20* (p=0.000, R^2=0.213)	+0.01* (p=0.000, R^2=0.120)
Upstream Section	+0.04 (p=0.007, R^2=0.030)	+1.90 (p=0.000, R^2=0.000)	0.00 (p=0.450, R^2=0.010)
Plateau Section	-0.02 (p=0.007, R^2=0.160)	+0.30 (p=0.000, R^2=0.094)	0.00 (p=0.000, R^2=0.020)
Downstream Section	+0.30* (p=0.000, R^2=0.324)	+4.20* (p=0.000, R^2=0.302)	+0.02 (p=0.000, R^2=0.000)
Flat Region	+0.44* (p=0.000, R^2=0.349)	+2.90* (p=0.000, R^2=0.164)	+0.02* (p=0.000, R^2=0.230)

Downstream Section; Table 2). This significant northward trend is even stronger in the Flat Region (0.44° latitude per decade; p=0.000, R^2=0.349; Figure 4 (a), Flat Region; Table 2). This regional analysis indicates that the slight northward trend of the whole meander (0.12° latitude per decade) is dominated by that of the meander downstream of the Plateau and, particularly, in the Flat Region.

In this study, we also investigate the meridional displacement trends of individual peaks and troughs of the meander between 1993 and 2020. We find that their decadal migration is not statistically significant, quite noisy, and of mixed signs (Table 3): some have moved northward (Trough 4 and Peak 2: 0.10° and 0.26° latitude per decade, respectively), some southward (Trough 1: -0.17° latitude per decade), while some are relatively stationary (Trough 2 and Peak 3: -0.02° and 0.03° latitude per decade, respectively). The most notable meridional trends over the 1993-2020 period, though not statistically significant, are observed in Trough 3 with a northward trend of 0.39° latitude per decade and Peak 4 with a southward trend of -0.31° latitude per decade (Table 3).

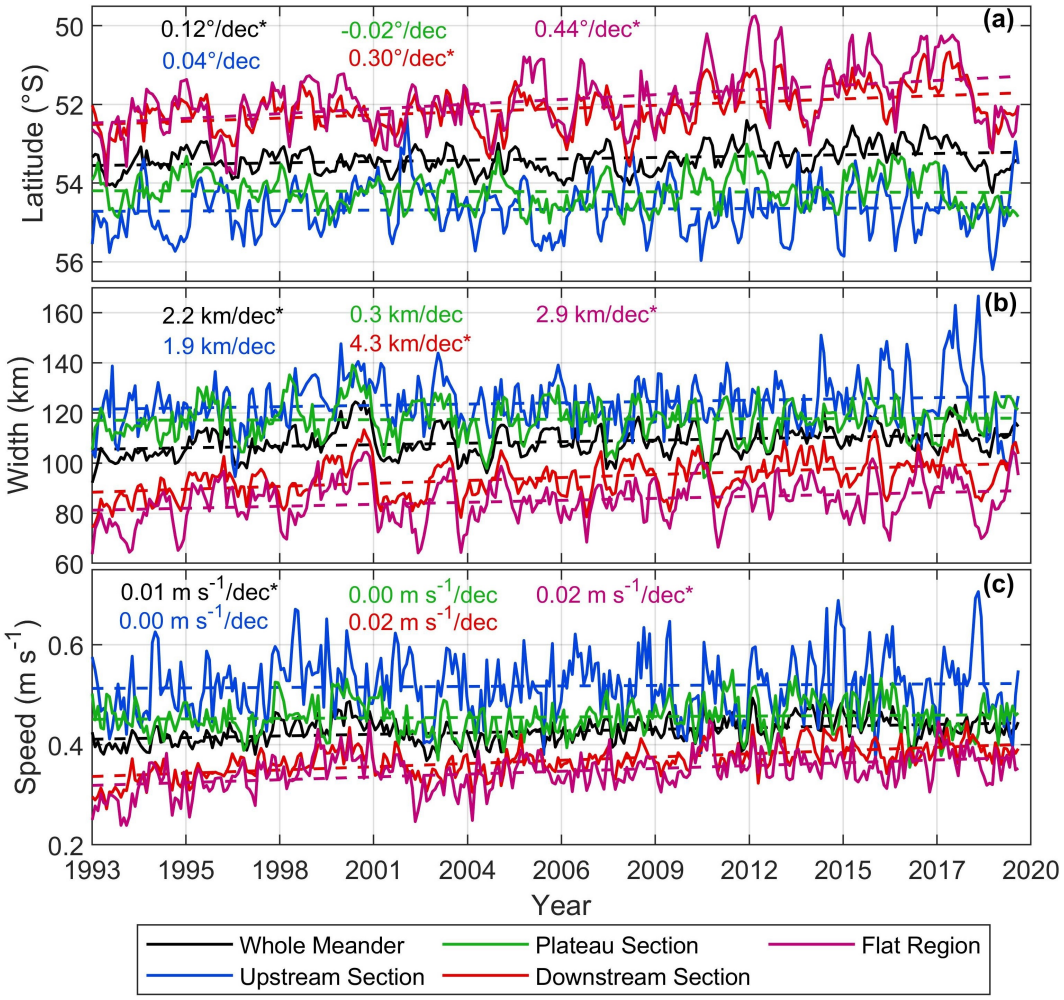

Figure 4. Monthly time series (solid lines) and corresponding linear trends (dashed lines) over the 1993-2020 period of the Campbell Plateau meander's (a) mean latitude position (degrees latitude per decade), (b) width (km per decade), and (c) geostrophic current speed ($m\ s^{-1}$ per decade). Positive trend values in the mean latitude position, width, and geostrophic current speed represent the northward movement, widening, and accelerating of the meander; while negative trends indicate the southward movement, narrowing, and decelerating of the meander. Statistically significant trends are indicated with '*'.

Table 3. Meridional displacement (latitude position) trends of the peaks and troughs of the Campbell Plateau meander in degree latitude per decade ($^\circ\ lat/dec$) based on the monthly data time series over the 1993-2020 period. Positive trend values indicate northward movements while negative trends indicate southward movements of peaks and troughs.

	Trough 1	Trough 2	Trough 3	Trough 4
Position ($^\circ\ lat/dec$)	-0.17 (p=0.052, R^2=0.018)	-0.02 (p=0.585, R^2=0.001)	+0.39 (p=0.159, R^2=0.024)	+0.10 (p=0.361, R^2=0.003)
	Peak 1	Peak 2	Peak 3	Peak 4
Position ($^\circ\ lat/dec$)	+0.05 (p=0.593, R^2=0.002)	+0.26 (p=0.000, R^2=0.122)	+0.03 (p=0.091, R^2=0.014)	-0.31 (p=0.001, R^2=0.035)

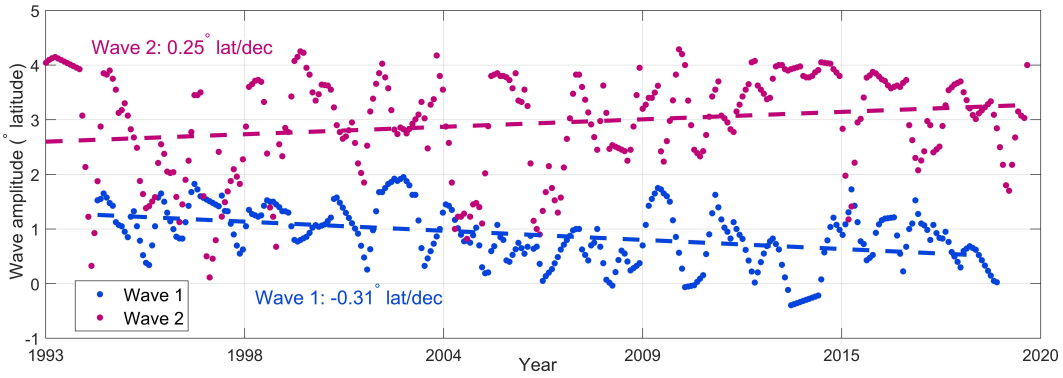

Figure 5. Monthly time series of the Campbell Plateau meander's wave amplitude in *degrees latitude* (° *lat*) at Wave 1 (blue dots) and Wave 2 (magenta dots) and corresponding linear trends in *degree* latitude per decade (° *lat*/*dec*) over the 1993-2020 period (dashed lines).

Based on the meridional displacement trends of the paired peaks and troughs, we also derive a time series of the meander amplitude in two places along its trajectory as half of the meridional distance between the selected pair of peaks and troughs and estimate the trends of these two wave amplitudes over the 1993-2020 period (Figure 5). Wave 1, composed of Trough 1 and Peak 2, is upstream of the Campbell Plateau, while Wave 2, composed of Peak 4 and Trough 4, is downstream of the Plateau (Figure 3). The trends of the wave amplitude at these two spots indicate a flattening of Wave 1 and flexing of Wave 2: the meander amplitude in Wave 1 has reduced by 0.31° latitude per decade, indicating that the meander is flattening upstream of the Plateau between 1993 and 2020 (Figure 5, Wave 1), while for Wave 2, the meander amplitude has increased by 0.25° latitude per decade, indicating that the meander has been steepening downstream of the Plateau (Figure 5, Wave 2).

3.3 Observed Changes in Meander Width

Over the 1993-2020 period, the mean width of the meander is 108 km (Figure 4 (b)). Upstream of the Campbell Plateau, the mean width is slightly wider (124 km for the Upstream Section and 117 km for the Plateau Section), while downstream of the Plateau, the mean width is narrower (94 km for the Downstream Section and 85 km for the Flat Region). This is consistent with research by Shao et al. (2015) showing reduced frontal widths downstream from significant topographic features such as the Campbell Plateau and the Kerguelen Plateau.

Based on our width definition (Figure 2 (b) and (c)), the whole meander has been significantly widening by 2.2 km per decade between 1993 and 2020 (Figure 4 (b); Table 2). Although each section of the meander has a widening trend, the Upstream and Plateau sections have exhibited a weaker widening than the sections downstream of the Plateau, and their trends are not statistically significant (Figure 4 (b); Table 2). By comparing the widening trend from the Downstream Section (4.2 km per decade) with that from the Flat Region (2.9 km per decade), we find that the Downstream Section contributes most to the overall widening trend (2.2 km per decade) over the 1993-2020 period (Table 2; Figure 4 (b)).

3.4 Observed Changes in Meander Speed

Based on the geostrophic current speed estimated from the AVISO data, we find the overall meander has been significantly accelerating by 0.01 $m\ s^{-1}$ per decade over

the 1993-2020 period, primarily in the Flat Region (Figure 4 (c); Table 2). Similar to the meridional displacement and widening trends, the Upstream and Plateau sections have almost no change in geostrophic current speed (0.00 $m\ s^{-1}$ per decade), while the Downstream Section and the Flat Region show an increase in speed (0.02 $m\ s^{-1}$ per decade) (Figure 4 (c); Table 2). However, only the acceleration in the Flat Region is significant (p=0.000, R^2=0.230; Table 2). Shi et al. (2021) report a similar average increase in surface eastward geostrophic velocities of 0.74±0.25 $cm\ s^{-1}$ *per century* (i.e., 0.00074±0.00025 $m\ s^{-1}$ per decade) between 48°S and 58°S for the entire Southern Ocean over the 1993-2019 period. More interestingly, the various datasets Shi et al. (2021) used (including the AVISO product) identify the area downstream of the Campbell Plateau as a hotspot for acceleration (Shi et al. (2021), Fig. 5 b). Their estimate of an acceleration of approximately 0.01 $m\ s^{-1}$ per decade (10 $cm\ s^{-1}$ *per century*) matches our estimate of 0.01 $m\ s^{-1}$ per decade (Figure 4 (c)). Peng et al. (2022) also identify this region as a hotspot for current speed acceleration. Although the overall speed trend is positive and significant, we see that there is large inter-annual and decadal variability in the monthly speed time series (Figure 4 (c)). Analysing the drivers behind this variability is beyond the scope of this study but would be worth investigating in future work.

4 Discussion

In this study, we use the AVISO absolute dynamic topography and geostrophic current velocities to identify the Campbell Plateau meander in the southwest Pacific Ocean (Figure 1) and estimate the decadal trends in its meridional displacement, width and geostrophic current speed over the 1993-2020 period (Figure 2 and 3 and 4 and 11). We find that the meander downstream of the Plateau and particularly over the abyssal plain has significant trends in its zonal position, width and speed, while the rest of the meander (upstream of and along the Campbell Plateau) has much weaker trends compared to downstream (Figure 4 and 11).

The Downstream Section and, particularly the Flat Region (defined in Table 1), indicate a significant northward displacement trend of 0.4° latitude per decade (Figure 4 (a)) between 1993 and 2020. This drives the whole meander to move northward by 0.12° latitude per decade on average. Similarly, the whole meander has been widening by 2.2 km per decade (Figure 4 (b)) and accelerating by 0.01 $m\ s^{-1}$ per decade (Figure 4 (c)) between 1993 and 2020, which are primarily due to trends in the Downstream Section (widening by 4.2 km per decade) and the Flat Region (accelerating by 0.02 $m\ s^{-1}$ per decade), respectively. The Upstream and Plateau sections do not contribute to the overall northward displacement, widening and accelerating trends of the whole meander (Table 2). Although the Upstream Section indicates a strong widening trend of 1.90 km per decade, it is not significant. The Plateau Section even has a southward displacement trend of -0.02° latitude per decade.

Here, we propose two hypotheses to explain the observed trends of the meander downstream of the Campbell Plateau: 1. Changes in the stability of the fronts and jets that compose the meander, and 2. changes in the South Pacific Gyre. In this discussion, we evaluate evidence for each of these hypotheses in turn.

4.1 Hypothesis 1: Changes in the Downstream Jet Stability

To explain the overall northward displacement of the whole meander, especially downstream of the Campbell Plateau, we hypothesise that changes in the stability properties of the jet could lead to a changing eddy field (Figure 6 (b) and (c)) and, therefore, the ability of the jet to meander downstream and potentially, the northward displacement of the meander downstream. To further examine this hypothesis, we investigate the distributions and trends of (1) mesoscale turbulent eddies, (2) background wind forcing, and

(3) the structure of the water column in the region. We also discuss how these distributions may be related to the width and speed trends of the meander.

4.1.1 (1) Changes in Eddy Kinetic Energy

We computer the Eddy Kinetic Energy (EKE) as EKE = $\frac{1}{2}[(u')^2+(v')^2]$, where u' and v' are the zonal and meridional geostrophic velocity anomalies compared to their 1993-2020 seasonally climatology mean values. Looking at the distribution and trends of EKE, we find that EKE increases in the whole meander (0.0010 $m^2\ s^{-2}$ per decade) with most of the signal in the Downstream Section (0.0014 $m^2\ s^{-2}$ per decade; Figure 6 (c)). Changes in eddy activity can both intensify and flatten the meandering of the currents (Williams et al., 2007; Abernathey & Cessi, 2014)

Overall, when trying to relate the spatial and temporal trend patterns of EKE in the Campbell Plateau region to the trends of the meander, we find that EKE patterns correspond to regions with significant trends in the width and geostrophic current speed trends of the meander.

The Upstream Section of the meander has the largest trend in width over the entire 1993-2020 period and the largest temporal-mean width (124 km; Figure 2 (b)). The widening trend of the Upstream Section is also not significant though it is relatively strong among the whole meander and its other sections (1.9 km per decade; Table 2). This matches that EKE in the Upstream Section is consistently the largest over the 1993-2020 period (larger than 0.02 $m^2\ s^{-2}$) and shows a strong increasing trend but it is not significant (0.0024 $m^2\ s^{-2}$ per decade, p=0.00, R^2=0.07; Figure 6 (c)). The significant widening trend of the Downstream Section drives the widening of the whole meander (Figure 2 (b)). Similar to the EKE trends in the Campbell Plateau region, the widening trend of the Flat Region contributes to about half of that of the Downstream Section and is comparative to that of the whole meander (Figure 2 (b)). Therefore, the EKE changes in the Campbell Plateau region could contribute to the widening trend of the meander between 1993 and 2020, especially downstream.

The trends in the EKE and geostrophic current speeds also show a notable alignment. Overall, we see that EKE in the Upstream Section is consistently the largest and indicates the strongest increasing trend but is not statistically significant; while EKE in the Downstream Section indicates the most significant increasing trend driving the overall significant increase of EKE in the whole meander (Figure 6). Although the Upstream Section does not show a trend in geostrophic current speed, it is still the largest over the 1993-2020 period (Figure 4 (c), Upstream Section), which matches that the largest EKE occurs in the Upstream Section between 1993 and 2020 (Figure 6, Upstream Section). While the Downstream Section does not show a significant trend in EKE, this trend is still strong, which is somewhat consistent with EKE trends of the Downstream Section (Figure 6, Downstream Section). The Flat Region shows the largest accelerating trend in geostrophic current speed and it is significant (Figure 4 (c)). This is also similar to EKE trends of the Flat Region (Figure 6, Flat Region). Therefore, the EKE changes in the Campbell Plateau region may account for the accelerating trend of the meander over the 1993-2020 period.

Recent work by Y. Zhang et al. (2021) on regional EKE trends in the Southern Ocean also highlights that the region downstream of the Campbell Plateau (180°W-150°W) is the only region characterised by a constant increase in EKE over the 1993-2019 period, which is consistent with our findings. Overall, we find that trends of EKE in the Campbell Plateau region strongly match the observed widening and accelerating trends of the meander. This suggests that EKE changes in the Campbell Plateau region over the 1993-2020 period may be linked with the observed trends in the width and geostrophic current speed.

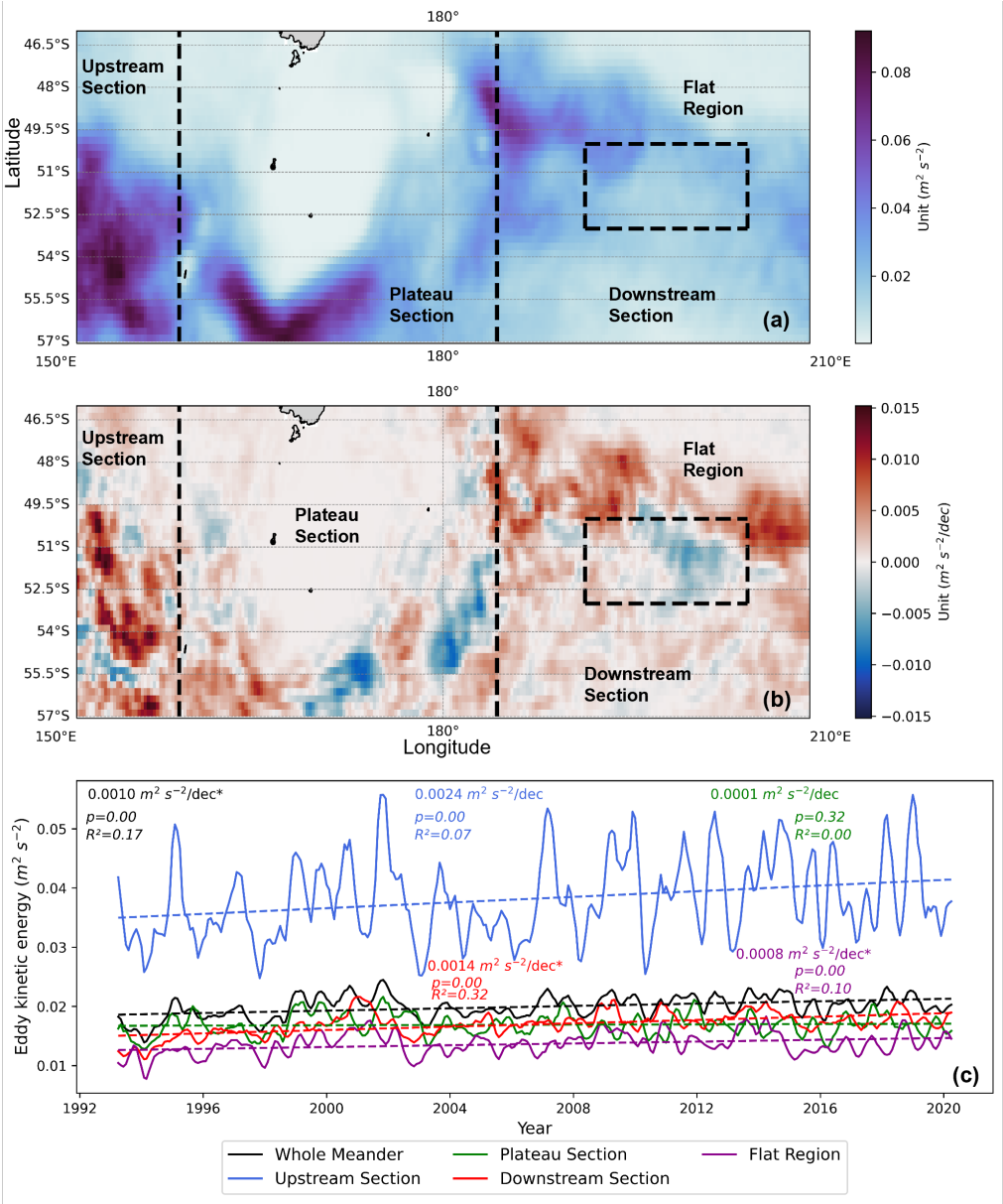

Figure 6. (a) Spatial distributions of mean EKE (m^2 s^{-2}) and (b) mean EKE decadal trend (m^2 s^{-2} per decade) over the 1993-2020 period in the Campbell Plateau region. (c) Monthly time series (solid lines) and corresponding linear trends (dashed lines) over the 1993-2020 period of EKE in m^2 s^{-2} per decade in different sections of the meander. The statistically significant trends are indicated with '*'.

4.1.2 (2) Changes in Wind Speeds

We now investigate changes in wind speeds over the 1993 to 2020 period to better understand their potential role in the meander changes.

We find a strengthening trend of the westerly winds in the whole meander and the Downstream Section. Since the zonal winds over the meander are dominated by the westerlies (red/blue colour in subplot (a) and (c) in Figure 7), the consequent Ekman transport should be northward. When the westerlies intensify over the 1993-2020 period, the northward Ekman transport should also intensify (Figure 7), suggesting a potential northward displacement of the meander. Hence, it is possible that changes in winds in this region have led to the northward displacement of the meander over the 1993-2020 period. However, we note that the wind speed trends in all the sections of the Campbell Plateau region are not statistically significant, especially the Downstream Section and the Flat Region (Figure 7 (e), Downstream Section and Flat Region).

However, we find contrasting patterns between the wind speed changes and amplitude changes of the meander upstream: in the Upstream Section, the zonal wind speeds indicate the strongest increase over the 1993-2020 period but the amplitude of the Upstream Section decreases and the meander upstream flattens (Figure 5 and 7 (e), Upstream Section). Thompson and Naveira Garabato (2014) and X. Zhang et al. (2023) have investigated the curvature changes (flexing) in the Southern Ocean standing meanders and propose that the standing meander's amplitude grows as a result of the stronger bottom flow caused by intensified wind forcing, inducing the flexing of the meander. It is also possible that the increased baroclinic flow of the meander downstream drives the flexing of the Downstream Section (Figure 5). While the intensifying wind speeds in the Upstream Section may increase the barotropic flow and lead to the flattening of the meander upstream, it is not clear if the observed increasing wind speed trends are sufficient to cause the northward shift in the meander's position, particularly downstream. The magnitude of wind speed changes necessary to significantly change the meander's latitude position remains uncertain.

As for the relationship between wind speed changes and meander's speed trends, according to the eddy saturation hypothesis (Straub, 1993; Meredith & Hogg, 2006), an increase in the westerly winds over the Southern Ocean would lead to an increase in Ekman transport, tilting the isopycnals and causing an increase in the baroclinicity of water masses. In turn, this would lead to an increase in EKE, causing the isopycnals to relax and ultimately, there would be no net wind-induced transport (Hogg & Blundell, 2006; Meredith & Hogg, 2006; D. Marshall et al., 2017) and so no direct acceleration of the meander. We note that the wind speed trend in the Flat Region is in contrast with the corresponding geostrophic current speed trend (Figure 4 and 7, Flat Region): The geostrophic current speed in the Flat Region shows the strongest and significant increasing trend, but the wind speed there shows a decreasing trend. Therefore, the wind changes in this region may not explain the acceleration of the meander between 1993 and 2020.

4.1.3 (3) Changes in Regional Hydrography

In addition to the EKE and wind speed, we also investigate changes in the regional hydrography in the Campbell Plateau region. More specifically, we look at changes in the oceanic thermal structure by analysing a gridded temperature product based on temperature profiles from Argo floats over the 2006-2022 period. We cannot extend the analysis to prior to 2006, as there were not enough Argo floats in the Southern Ocean to derive reliable statistics before 2006.

We find that almost all the isotherms (2.0 ℃-11.0 ℃) within all depths slightly move southward from the 2006-2010 period (blue) to the 2016-2019 period (cyan) in the Campbell Plateau region (Figure 8). Particularly in the upper 100 m, the isotherms (5.0 ℃-

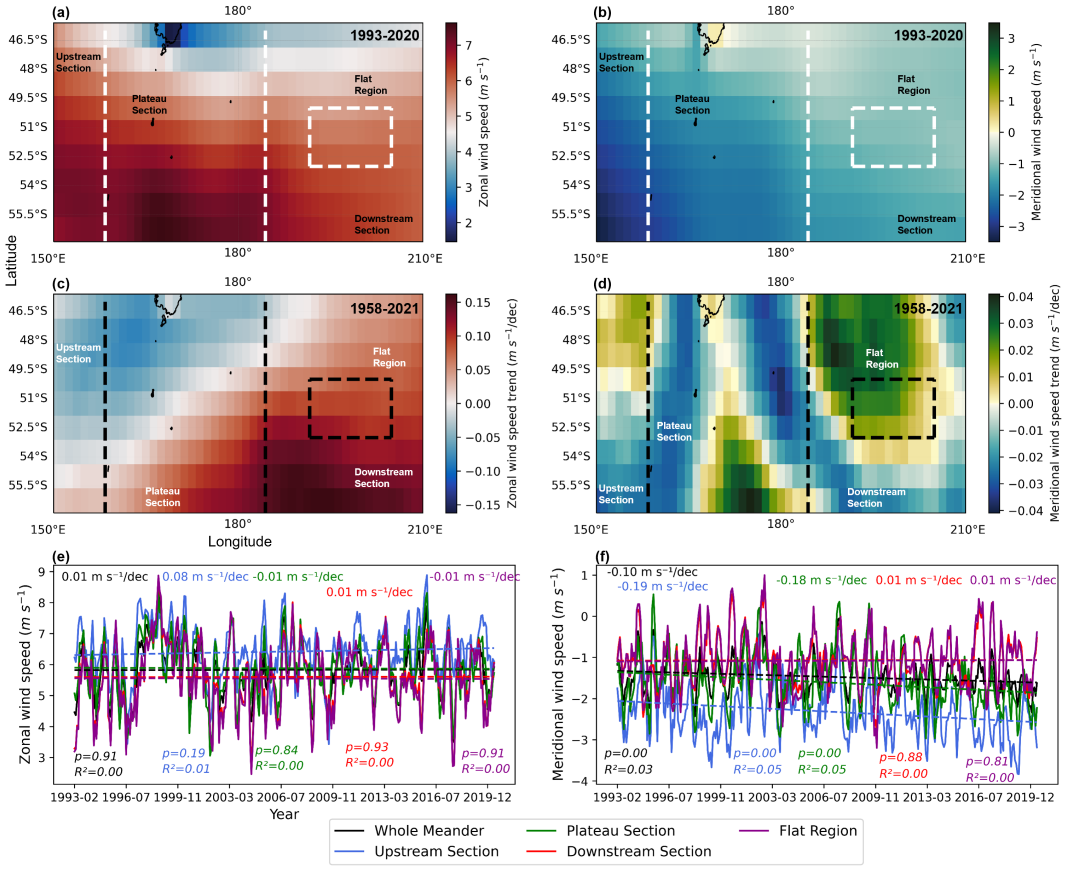

Figure 7. Spatial distributions of (a) zonal and (b) meridional mean wind speed over the 1993-2020 period in $m\ s^{-1}$ in the Campbell Plateau region. Positive zonal and meridional winds are eastward and northward, respectively. Spatial distributions of the decadal mean trends of (c) zonal and (d) meridional wind speed over the 1958-2021 period in $m\ s^{-1}/dec$ ($m\ s^{-1}$ per decade) in the Campbell Plateau region. Monthly time series (solid lines) and corresponding linear trends (dashed lines) over the 1993-2020 period of (e) zonal and (f) meridional wind speed in $m\ s^{-1}/dec$ ($m\ s^{-1}$ per decade) in different sections of the Campbell Plateau region. None of the trends are statistically significant.

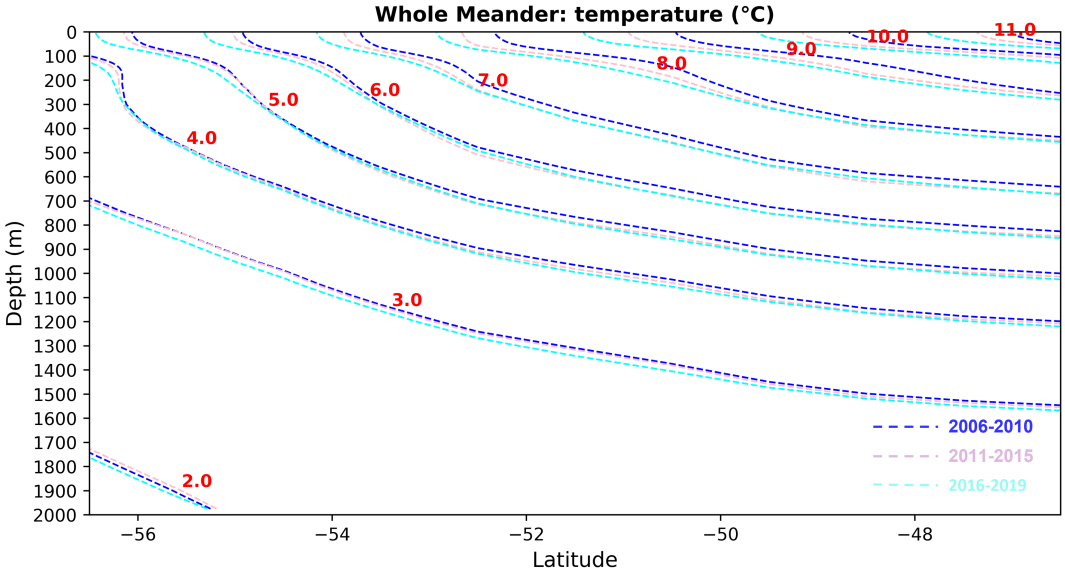

Figure 8. Argo mean ocean temperature contour (isotherms) section plot for 2006-2010 (blue), 2011-2015 (pink) and 2016-2020 (cyan) in the Campbell Plateau region (57°S-46°S and 150°E to 210°E). The values of 2011-2015 mean temperature contours are annotated in red.

11.0 ℃) moved southward sharply from the 2006-2010 period to the 2016-2019 period, consistent with ongoing global warming. However, the tilt of these isotherms, which is related to both the temporal-mean geostrophic current speed and the baroclinic stability of the water column, does not change significantly over the 2006-2022 period (Figure 8). The ocean temperature in the Campbell Plateau region indicates overall warming across the upper 2000 m and latitudinal range, with a stronger signal in the north and in the upper ocean (54°S-57°S and 0-1000 m depth; Figure 9 (a)). These warming trends are stronger in the Upstream and Plateau sections (Figure 9 (b) and (c)). Although the Downstream Section and the Flat Region show overall warming trends, they indicate small localised subsurface cooling trends (Figure 9 (d) and (e)).

The southward displacement of the isotherms in the Campbell Plateau region contrasts with the northward shift of the meander and does not explain this shift. The significant regional differences in the rate and structure of the ocean warming point to increasing temperature gradients: warming trends are clearly strongest in the Upstream Section, with warming rates greater than 0.4 ℃ per decade down to 1000 m depth in the central latitudes (Figure A1). Warming rates are more moderate over the remaining regions, with cooling observed south of 52°S in both the Downstream Section and the Flat Region (Figure A1). The contrasting warming-cooling in the Downstream Section and the Flat Region suggests an increase in the local temperature gradients, which, through the thermal wind relationship, suggests an increase in the zonal geostrophic current speed. The observed increase in the meridional temperature gradients overlaps where the highest trends are observed in meander position, width and speed (Figure 4 and 9). Therefore, the movement of the isotherms in the Campbell Plateau region may not explain the overall northward displacement of the meander between 1993 and 2020.

However, we find that the warming trends in the Campbell Plateau region match the location of the accelerating trends of the meander. According to Shi et al. (2021), oceanic warming dominates this acceleration. Specifically, the increasing heat gain in the downwelling regions north of the Subantarctic Front largely contributes to this zonal acceleration on the northern flank of the ACC due to the increased baroclinicity (Shi et

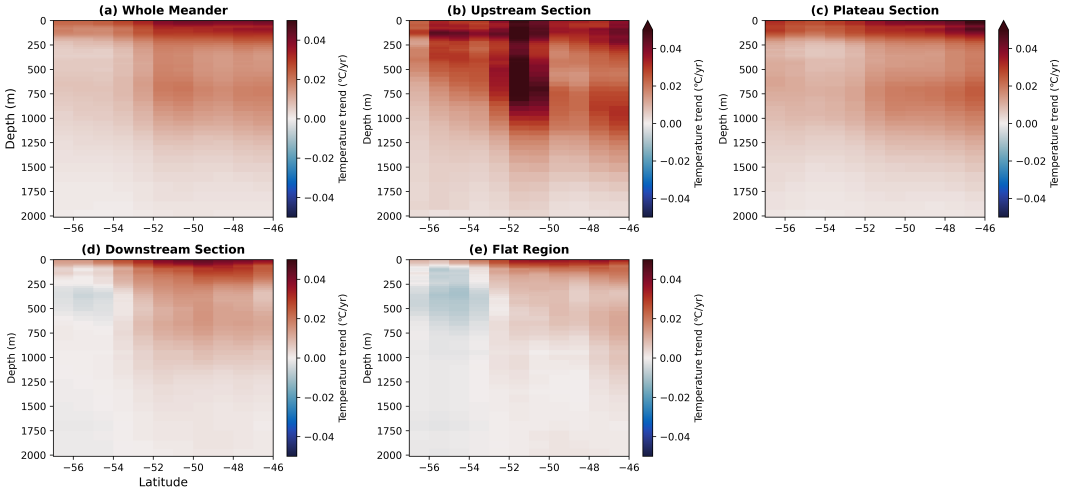

Figure 9. Section plot of the annual trends of Argo ocean temperatures in degrees Celsius per year (°C/yr) over the 2006-2020 period in different sections of the Campbell Plateau region: (a) Whole Meander, (b) Upstream Section, (c) Plateau Section, (d) Downstream Section and (e) Flat Region.

al., 2021). Interestingly, the only area marked by a significant acceleration in Shi et al. (2021) corresponds to the Downstream Section in our study, which is also the only region identified in this study with an increasing meridional temperature gradient (Figure 9 (d) and A1 (c)). The temperature gradient changes in the Downstream Section are consistent with the observed northward displacement of the meander downstream (Figure 4 (a), Downstream Section), and ongoing oceanic warming may contribute to driving the observed trends.

Overall, our results indicate that the increasing EKE trends over the 1993-2020 period could potentially explain the observed widening and acceleration of the meander, particularly in the Downstream Section of the meander; strengthening westerly winds may partially explain the observed northward displacement of the meander; and the changing hydrography with increasing meridional temperature gradients might explain the acceleration of the meander, especially downstream.

To explain the changes in meander width, we would need to know about local trends in current transport. However, there is no dataset that we are aware of to do such an analysis in the Campbell Plateau region. While there is no detected or modelled trend in the net transport of the ACC in regions with long observational time series (Meredith et al., 2011; Koenig et al., 2014; Xu et al., 2020), trends in the individual Southern Ocean fronts (e.g., Chouaib et al. (2006)) such as the Campbell Plateau meander cannot be ruled out. Such trends could potentially contribute to the widening of the Campbell Plateau meander fronts through processes such as enhanced baroclinic instability downstream of the Plateau and increased eddy occurrence (Thompson et al., 2010). Such dynamic adjustments could affect the vertical and horizontal structures of the meander, including its width. Therefore, we can only speculate that changes in the volume transport are potentially driving the widening trend of the meander.

Follow-up work on the meander width should involve improving the width definition and testing the sensitivity of previously derived widening trends to different width definitions. The potential consequences of changes in the meander width would also be worth investigating. For example, the impacts of width changes on cross-frontal transport are relevant across many research fields including the anthropogenic heat and car-

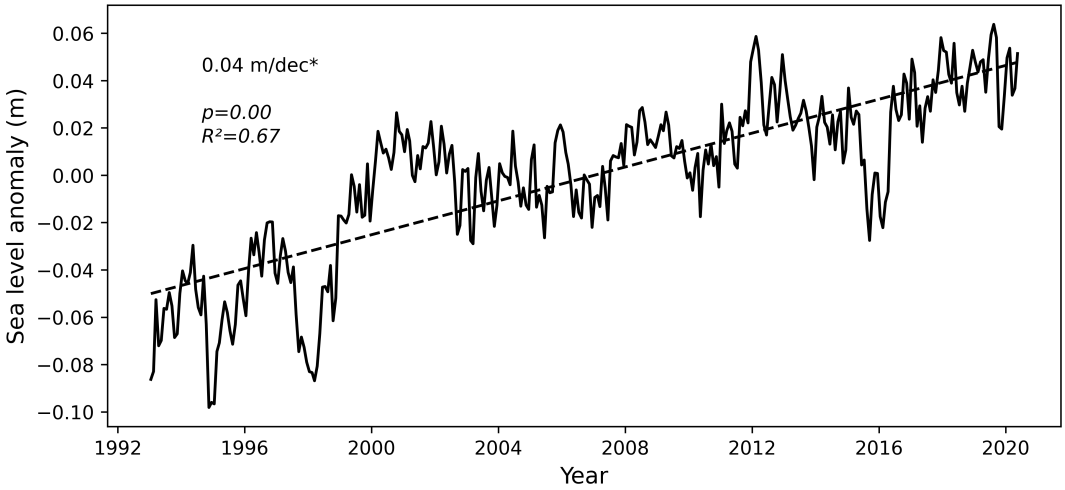

Figure 10. Monthly time series (solid line) of sea level anomaly (SLA) (m) and corresponding linear trend (dashed line) in meters per decade (m/dec) over the 1993-2020 period. SLA is estimated at the centre longitude of 190°E (170°W) over the longitudes of 150°E to 70°W (290°E) and latitudes of 38°S to 42°S to cover the South Pacific Gyre and the seasonal cycle is removed based on Roemmich et al. (2007). '*' indicates the trend is statistically significant.

bon budgets, tracer cycles, upwelling in the Southern Ocean, and even habitat and ecosystem changes (e.g., Hogg et al. (2008); Thompson and Sallée (2012); Barthel et al. (2017); Foppert et al. (2017); Murphy et al. (2021)).

4.2 Hypothesis 2: Changes in the South Pacific Gyre

Changes in the South Pacific Gyre may be linked to the observed changes in the Campbell Plateau meander. As a proxy for the South Pacific Gyre strength, we choose to use the AVISO sea level anomaly (SLA) at the central longitude of 190°E (170°W) spanning from 150°E to 290°E (70°W) averaged over the latitude region of 38°S-42°S with the seasonal cycle removed (Figure 10; Roemmich et al. (2007)). This "gyre index" is strongly and positively correlated with the velocity of the South Pacific Gyre (Roemmich et al., 2007). Over the 1993-2020 period, we see that the SLA indicates a significant increasing trend of 0.04 m per decade (p=0.00, R^2=0.67; Figure 10). This suggests that the Gyre velocity is increasing and thus, that the South Pacific Gyre is strengthening between 1993 and 2020, implying a general contraction of the gyre boundary.

We hypothesize that the northward shift of the meander is due to changes in the interaction between the South Pacific Gyre and ACC jets. Since the zonal wind speeds have been increasing from 1993 to 2020 (Figure 7), they are likely to drive a stronger gyre and enhance the northward Ekman transport, shifting the southern boundary of the Gyre northward (Roemmich et al., 2007). A northward shift in the southern boundary of the Gyre could explain the northward displacement of the Downstream Section of the meander. It is also possible that this Ekman transport is driving changes in the meandering pattern downstream of the Plateau by impacting the position of the Gyre. The subtropical gyre in the South Pacific Ocean has been accelerating and intensifying since the early 1990s due to the changes in wind stress in this area (Cai et al., 2005; Saenko et al., 2005; Qiu & Chen, 2006; Roemmich et al., 2007; C. Liu & Wu, 2012).

4.3 Topography

In this study, we also briefly discuss how topography impacts the widening trends of the meander and its various sections. The topography of the Campbell Plateau impacts the width of the meander and potentially its trends by strongly constraining the flow of parts of the meander, for example in the Upstream and Plateau sections. There, the widening trends, while positive are not statistically significant (Table 2); while the Downstream Section, which is not constrained by the topography of the Plateau, has the strongest widening trend (Figure 4). This matches our observations that the mean width of the Campbell Plateau meander decreases from the Upstream Section (124 km) to the Downstream Section (94 km; Figure 4 (b)). These topography-induced narrower frontal widths are possibly caused by the sharpening of jets or the decrease in the distance between jet cores (Shao et al., 2015). Furthermore, in the Downstream Section, where there is almost no topography constraining the flow (Figure 3, Downstream Section), the fronts are separated into more jets rather than having one dominant core (Thompson & Sallée, 2012; X. Zhang et al., 2023), which could explain the widening of the meander.

4.4 Variations in Southern Ocean Meanders

While there are few studies on trends of the Southern Ocean meanders (e.g.,Thompson and Naveira Garabato (2014)), our findings for the Campbell Plateau meander can be compared with a recent study on the Agulhas-Kerguelen standing meander by Meyer et al. (2023). They analysed the characteristics and trends of the Agulhas-Kerguelen standing meander over the 1993-2019 period using satellite sea surface height data and similar meander identification methods. Interestingly, the overall trends of both meanders, despite different geographical locations and slightly different dynamical regimes, are similar: no southward migration of the standing meanders and both meanders are widening and accelerating. Observing similar trends in position, wave amplitude, width, and geostrophic current speed for these two meanders suggests that the changes and impacts of these trends on cross-frontal transport of heat, carbon, and other tracers, might not be limited to only one Southern Ocean meander but potentially to several meanders in the Southern Ocean.

Changes in the amplitude of the Southern Ocean standing meanders could play a significant role in the horizontal and vertical energy transport as well as eddy fluxes. The flexing of standing meanders along the ACC may help transport the wind-induced momentum input to the ocean bottom, which is thought to be significant in regulating how ACC reacts to wind (Thompson & Naveira Garabato, 2014; X. Zhang et al., 2023). Flexing of the meander may also result in the intensification of transient eddies and their associated fluxes, which consequently result in a relaxation of isopycnals downstream of the topography within the meander (Abernathey & Cessi, 2014).

5 Conclusions

Standing meanders are an important feature of the Southern Ocean, being sites of enhanced meridional and vertical exchange, yet their response to climate change is unclear. In this study, we identified and characterised the Campbell Plateau meander, located south of New Zealand in the Southern Ocean, over the 1993-2020 period using satellite observations. We identified the position and estimated the associated trends in the meander's latitude position, amplitude, width, and surface geostrophic current speed (see Figure 11 for the summary). Between 1993 and 2020, the position of the Campbell Plateau meander remained relatively stationary, except for a section downstream of the Campbell Plateau moving northward by 0.4° latitude (approximately 40 km) per decade. The meander has been flattening at the western edge of the Plateau while flexing at the eastern edge. Moreover, the meander has been significantly widening (2 km per decade) and its surface geostrophic current speed has been increasing (0.01 $m\ s^{-1}$ per decade), in par-

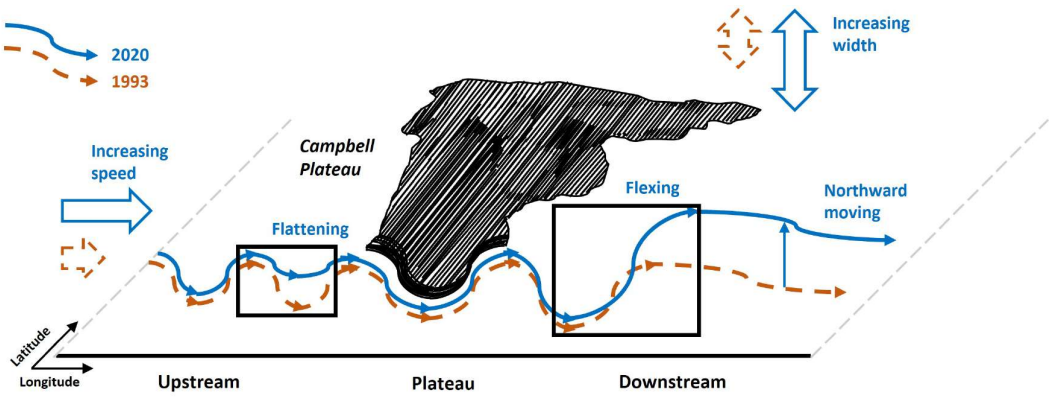

Figure 11. Schematic illustrating the trends of the Campbell Plateau meander's position, flattening and flexing of the meander's shape, widening of the meander in some parts, and increasing geostrophic current speed over the 1993-2020 period. The Campbell Plateau is represented by the shaded area. This schematic is based on and modified from FIG. 16 in X. Zhang et al. (2023).

ticular downstream of the Plateau. While the increasing geostrophic current speed values match existing literature, they are close to the instrument error threshold and potentially not statistically significant when the error of the instrument is taken into account (Taburet et al., 2019). Interestingly, despite differences in geographical settings and dynamical regimes, the Campbell Plateau meander and the Agulhas-Kerguelen standing meander share similar trends in their position, amplitude, width, and surface geostrophic current speed. We hypothesise that changes in the downstream jet stability and changes in the South Pacific Gyre may explain the observed trends of the meander in its meridional displacement, width and geostrophic current speed. We find that significant increasing trends in eddy kinetic energy and of the South Pacific Gyre index over the 1993-2020 period, especially downstream of the Campbell Plateau, support our findings. The warming trends of the water column in the Campbell Plateau region are likely to explain part of the acceleration of the meander while increasing zonal wind speeds do not seem to play a role in the width and speed trends of the meander. Future work should investigate the drivers behind the changes in the Campbell Plateau meander's amplitude and resulting dynamic adjustments, along with the impacts of these observed trends on the cross-frontal transport of the Antarctic Circumpolar Current.

Acronyms

ACC Antarctic Circumpolar Current
ADT Absolute Dynamic Topography

AVISO Archiving, Validation and Interpretation of Satellite Oceanographic
EKE Eddy Kinetic Energy
SLA Sea Level Anomaly
SSH Sea Surface Height
SST Sea Surface Temperature

6 Data and Software Availability Statements

ADT and geostrophic current velocity data: The satellite altimetry absolute dynamic topography data as well as zonal and meridional surface geostrophic current velocities data (Product: Global Ocean Gridded L 4 Sea Surface Heights And Derived Variables Reprocessed 1993 Ongoing) used for identifying, characterising and analysing the trends of the Campbell Plateau meander as well as analysing the trends of the end kinetic energy in the Campbell Plateau region over the 1993-2020 period in the study are publicly available (last access: December 2023) at Marine Data Store, European Union Copernicus Marine Environment Monitoring Service via the website at `https://data.marine.copernicus.eu/product/SEALEVEL_GLO_PHY_L4_MY_008_047/services`.

Bathymetric data: The bathymetric data used for mapping the local bathymetry in the Campbell Plateau region in the study are publicly available (last access: December 2023) at Global Multi-Resolution Topography GridServer Web Service via the website at `https://www.gmrt.org/services/gridserverinfo.php#!/services/getGMRTGrid` (Ryan et al., 2009).

Wind speeds data: The JRA-55 zonal and meridional wind speeds used for analysing the spatial and temporal trends of the zonal and meridional wind speeds over the 1993-2020 period in the Campbell Plateau region are publicly available (last access: December 2023) at the JRA-55 project via the website at `https://jra.kishou.go.jp/JRA-55/index_en.html`.

SLA data: The SLA data used for analysing the trends of the South Pacific Gyre index in the South Pacific Ocean are publicly available (last access: August 2023) via the website at `https://www.aviso.altimetry.fr/en/data/products/sea-surface-height-products/global/along-track-sea-level-anomalies-l2p.html`.

Argo data: The Argo data used for analysing the oceanic thermal structure of the Campbell Plateau meander are publicly available (last access: December 2023) via the website at `https://sio-argo.ucsd.edu/RG_Climatology.html`).

Software: MATLAB R2020a under the University of Tasmania License for students (MathWorks, 2020) used for analysing the characteristics and trends of the Campbell Plateau meander is available for students who currently study at the University of Tasmania with an individual license number via the website at `https://au.mathworks.com/academia/tah-portal/university-of-tasmania-30924569.html`. JupyterLab 3.4.4 (Anaconda3) (*JupyerLab 3.4.4*, 2023) used for analysing the trends of eddy kinetic energy, wind speeds, Argo temperature and sea level anomaly in the Campbell Plateau region is publicly available via the website at `https://www.anaconda.com/download`.

Acknowledgments

We are thankful to the University of Tasmania that provided support to conduct this research. XL acknowledges support from the Australian Research Council Centre of Excellence for Climate Extremes and the Institute for Marine and Antarctic Studies for his Honours year. XL and AM are supported by the Australian Research Council (ARC) Centre of Excellence of Climate Extremes (CLEX; ARC Grant No. CE170100023). CC acknowledges financial support from the Centre for Southern Hemisphere Ocean Research

(CSHOR). We thank two anonymous assessors from the Institute for Marine and Antarctic Studies for their feedback on this work. We also thank Xihan Zhang and Stuart Corney from the Institute for Marine and Antarctic Studies for their comments on this paper. This study has been conducted using E.U. Copernicus Marine Service Information. These data were collected and made freely available by the International Argo Program and the national programs that contribute to it (`https://argo.ucsd.edu`, `https://www.ocean-ops.org`). The Argo Program is part of the Global Ocean Observing System. Open access publishing facilitated by the University of Tasmania, as part of the Wiley-University of Tasmania agreement via the Council of Australian University Librarians.

Appendix A Argo Mean Ocean Temperature Contours in Four Sections of the Campbell Plateau Region

References

Abernathey, R., & Cessi, P. (2014). Topographic enhancement of eddy efficiency in baroclinic equilibration. *Journal of Physical Oceanography*, *44*(8), 2107–2126.

Argo. (2023). *Roemmich-gilson argo climatology* [dataset]. Scripps Institution of Oceanography. Retrieved from `https://sio-argo.ucsd.edu/RG_Climatology.html` doi: 10.17882/42182

AVISO. (2023). *Aviso along-track sea level anomalies level-2+ (l2p)* [dataset]. AVISO+. Retrieved from `https://www.aviso.altimetry.fr/en/data/products/sea-surface-height-products/global/along-track-sea-level-anomalies-l2p.html`

Bachman, S. D., Taylor, J., Adams, K., & Hosegood, P. (2017). Mesoscale and submesoscale effects on mixed layer depth in the southern ocean. *Journal of Physical Oceanography*, *47*(9), 2173–2188.

Barthel, A., Hogg, A. M., Waterman, S., & Keating, S. (2022). Baroclinic control of southern ocean eddy upwelling near topography. *Geophysical Research Letters*, e2021GL097491.

Barthel, A., McC. Hogg, A., Waterman, S., & Keating, S. (2017). Jet–topography interactions affect energy pathways to the deep southern ocean. *Journal of Physical Oceanography*, *47*(7), 1799–1816.

Bindoff, N. L., Cheung, W. W., Kairo, J. G., Arístegui, J., Guinder, V. A., Hallberg, R., ... Williamson, P. (2019). Changing ocean, marine ecosystems, and dependent communities. In H.-O. Pörtner et al. (Eds.), *Ipcc special report on the ocean and cryosphere in a changing climate* (pp. 447–587). Cambridge, UK and New York, NY, USA: Cambridge University Press. Retrieved from `https://doi.org/10.1017\%2F9781009157964.007` doi: 10.1017/9781009157964.007

Brady, R. X., Maltrud, M. E., Wolfram, P. J., Drake, H. F., & Lovenduski, N. S. (2021). The influence of ocean topography on the upwelling of carbon in the southern ocean. *Geophysical Research Letters*, *48*(19), e2021GL095088.

Cai, W., Shi, G., Cowan, T., Bi, D., & Ribbe, J. (2005). The response of the southern annular mode, the east australian current, and the southern mid-latitude ocean circulation to global warming. *Geophysical Research Letters*, *32*(23).

Carter, L., & Wilkin, J. (1999). Abyssal circulation around new zealand—a comparison between observations and a global circulation model. *Marine Geology*, *159*(1-4), 221–239.

Chapman, C. C. (2014). Southern ocean jets and how to find them: Improving and comparing common jet detection methods. *Journal of Geophysical Research: Oceans*, *119*(7), 4318–4339.

Chapman, C. C. (2017). New perspectives on frontal variability in the southern ocean. *Journal of Physical Oceanography*, *47*(5), 1151–1168.

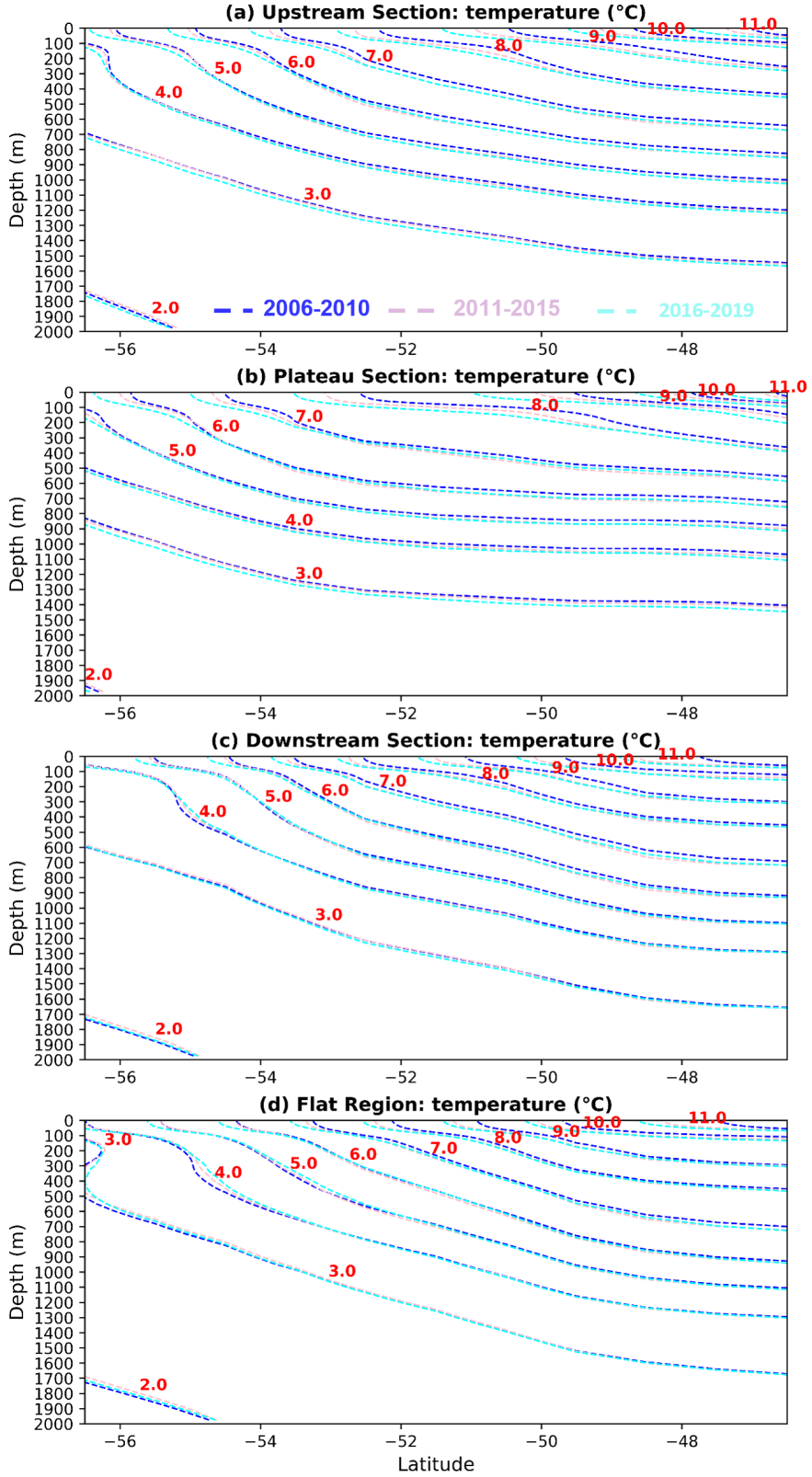

Figure A1. Argo mean ocean temperature contour section plot for 2006-2010 (blue), 2011-2015 (pink) and 2016-2020 (cyan) in different sections of the Campbell Plateau region: (a) Upstream Section, (b) Plateau Section, (c) Downstream Section and (d) Flat Region. The values of 2011-2015 mean temperature contours are annotated in red.

Chapman, C. C., Hogg, A. M., Kiss, A. E., & Rintoul, S. R. (2015). The dynamics of southern ocean storm tracks. *Journal of Physical Oceanography*, *45*(3), 884–903.

Chapman, C. C., Lea, M.-A., Meyer, A., Sallée, J.-B., & Hindell, M. (2020). Defining southern ocean fronts and their influence on biological and physical processes in a changing climate. *Nature Climate Change*, *10*(3), 209–219.

Chapman, C. C., & Sallée, J.-B. (2017). Isopycnal mixing suppression by the antarctic circumpolar current and the southern ocean meridional overturning circulation. *Journal of Physical Oceanography*, *47*(8), 2023–2045.

Chouaib, N., Stoehr, F., & Provost, C. (2006). Variability of the subantarctic and polar fronts in the drake passage as deduced from altimetry. *Journal of marine research*, *64*(5), 669–693.

CMEMS. (2023). *Global ocean gridded l4 sea surface heights and derived variables reprocessed (1993-ongoing)* [dataset]. European Union Copernicus Marine Environment Monitoring Service. Retrieved from `https://data.marine.copernicus.eu/product/SEALEVEL_GLO_PHY_L4_MY_008_047` doi: 10.48670/moi-00148

Cyriac, A., Meyer, A., Phillips, H. E., & Bindoff, N. L. (2023). Observations of internal wave interactions in a southern ocean standing meander. *Journal of Physical Oceanography*.

Deacon, G. E. R. (1937). The hydrology of the southern ocean. *Discovery Rep.*, *15*, 3–122.

Dong, S., Sprintall, J., & Gille, S. T. (2006). Location of the antarctic polar front from amsr-e satellite sea surface temperature measurements. *Journal of Physical Oceanography*, *36*(11), 2075–2089.

Donohue, K., Tracey, K., Watts, D., Chidichimo, M. P., & Chereskin, T. (2016). Mean antarctic circumpolar current transport measured in drake passage. *Geophysical Research Letters*, *43*(22), 11–760.

Dove, L. A., Balwada, D., Thompson, A. F., & Gray, A. R. (2022). Enhanced ventilation in energetic regions of the antarctic circumpolar current. *Geophysical Research Letters*, *49*(13), e2021GL097574.

Dove, L. A., Thompson, A. F., Balwada, D., & Gray, A. R. (2021). Observational evidence of ventilation hotspots in the southern ocean. *Journal of Geophysical Research: Oceans*, *126*(7), e2021JC017178.

Foppert, A., Donohue, K. A., Watts, D. R., & Tracey, K. L. (2017). Eddy heat flux across the antarctic circumpolar current estimated from sea surface height standard deviation. *Journal of Geophysical Research: Oceans*, *122*(8), 6947–6964.

Forcén-Vázquez, A., Williams, M. J., Bowen, M., Carter, L., & Bostock, H. (2021). Frontal dynamics and water mass variability on the campbell plateau. *New Zealand Journal of Marine and Freshwater Research*, *55*(1), 199–222.

Freeman, N. M., Lovenduski, N. S., & Gent, P. R. (2016). Temporal variability in the antarctic polar front (2002–2014). *Journal of Geophysical Research: Oceans*, *121*(10), 7263–7276.

Frölicher, T. L., Sarmiento, J. L., Paynter, D. J., Dunne, J. P., Krasting, J. P., & Winton, M. (2015). Dominance of the southern ocean in anthropogenic carbon and heat uptake in cmip5 models. *Journal of Climate*, *28*(2), 862–886.

Fu, L.-L., Chelton, D. B., Le Traon, P.-Y., & Morrow, R. (2010). Eddy dynamics from satellite altimetry. *Oceanography*, *23*(4), 14–25.

Gille, S. T. (2014). Meridional displacement of the antarctic circumpolar current. *Philosophical Transactions of the Royal Society A: Mathematical, Physical and Engineering Sciences*, *372*(2019), 20130273.

Gille, S. T., & Kelly, K. A. (1996). Scales of spatial and temporal variability in the southern ocean. *Journal of Geophysical Research: Oceans*, *101*(C4), 8759–8773.

Gille, S. T., Yale, M. M., & Sandwell, D. T. (2000). Global correlation of mesoscale ocean variability with seafloor roughness from satellite altimetry. *Geophysical Research Letters*, *27*(9), 1251–1254.

Gordon, A. (1972). The australian-new zealand sector. *Antarct. Res. Ser.*, *19*.

Graham, R. M., De Boer, A. M., Heywood, K. J., Chapman, M. R., & Stevens, D. P. (2012). Southern ocean fronts: Controlled by wind or topography? *Journal of Geophysical Research: Oceans*, *117*(C8).

Heath, R. (1981). Oceanic fronts around southern new zealand. *Deep Sea Research Part A. Oceanographic Research Papers*, *28*(6), 547–560.

Hogg, A. M. C., & Blundell, J. R. (2006). Interdecadal variability of the southern ocean. *Journal of physical oceanography*, *36*(8), 1626–1645.

Hogg, A. M. C., Meredith, M. P., Blundell, J. R., & Wilson, C. (2008). Eddy heat flux in the southern ocean: Response to variable wind forcing. *Journal of Climate*, *21*(4), 608–620.

Hughes, C. W. (2005). Nonlinear vorticity balance of the antarctic circumpolar current. *Journal of Geophysical Research: Oceans*, *110*(C11).

Hughes, C. W., & Ash, E. R. (2001). Eddy forcing of the mean flow in the southern ocean. *Journal of Geophysical Research: Oceans*, *106*(C2), 2713–2722.

Hughes, C. W., & Wilson, C. (2008). Wind work on the geostrophic ocean circulation: An observational study of the effect of small scales in the wind stress. *Journal of Geophysical Research: Oceans*, *113*(C2).

Jupyerlab 3.4.4 [software]. (2023). Anaconda Inc. Retrieved from `https://www.anaconda.com/download`

Killworth, P. D. (1992). An equivalent-barotropic mode in the fine resolution antarctic model. *Journal of Physical Oceanography*, *22*(11), 1379–1387.

Klocker, A. (2018). Opening the window to the southern ocean: The role of jet dynamics. *Science advances*, *4*(10), eaao4719.

Koenig, Z., Provost, C., Ferrari, R., Sennéchael, N., & Rio, M.-H. (2014). Volume transport of the a ntarctic c ircumpolar c urrent: Production and validation of a 20 year long time series obtained from in situ and satellite observations. *Journal of Geophysical Research: Oceans*, *119*(8), 5407–5433.

Langlais, C., Lenton, A., Matear, R., Monselesan, D., Legresy, B., Cougnon, E., & Rintoul, S. (2017). Stationary rossby waves dominate subduction of anthropogenic carbon in the southern ocean. *Scientific reports*, *7*(1), 1–10.

Langlais, C., Rintoul, S., & Schiller, A. (2011). Variability and mesoscale activity of the southern ocean fronts: Identification of a circumpolar coordinate system. *Ocean Modelling*, *39*(1-2), 79–96.

Lapeyre, G. (2009). What vertical mode does the altimeter reflect? on the decomposition in baroclinic modes and on a surface-trapped mode. *Journal of Physical Oceanography*, *39*(11), 2857–2874.

Liu, C., & Wu, L. (2012). An intensification trend of south pacific mode water subduction rates over the 20th century. *Journal of Geophysical Research: Oceans*, *117*(C7).

Liu, X. (2022). *Characteristics and trends of the campbell plateau meander in the southern ocean* (Honours thesis, University of Tasmania). doi: 10.25959/100.00047676

Llort, J., Langlais, C., Matear, R., Moreau, S., Lenton, A., & Strutton, P. G. (2018). Evaluating southern ocean carbon eddy-pump from biogeochemical-argo floats. *Journal of Geophysical Research: Oceans*, *123*(2), 971–984.

Lu, J., & Speer, K. (2010). Topography, jets, and eddy mixing in the southern ocean. *Journal of Marine Research*, *68*(3-4), 479–502.

Lumpkin, R., & Speer, K. (2007). Global ocean meridional overturning. *Journal of Physical Oceanography*, *37*(10), 2550–2562.

Marshall, D., Ambaum, M. H., Maddison, J. R., Munday, D. R., & Novak, L. (2017). Eddy saturation and frictional control of the antarctic circumpolar

current. *Geophysical research letters*, *44*(1), 286–292.

Marshall, J., & Speer, K. (2012). Closure of the meridional overturning circulation through southern ocean upwelling. *Nature geoscience*, *5*(3), 171–180.

MathWorks. (2020). *Matlab version: R2020a* [software]. The MathWorks Inc. Retrieved from `https://au.mathworks.com/academia/tah-portal/university-of-tasmania-30924569.html`

Meijer, J. J., Phillips, H. E., Bindoff, N. L., Rintoul, S. R., & Foppert, A. (2022). Dynamics of a standing meander of the subantarctic front diagnosed from satellite altimetry and along-stream anomalies of temperature and salinity. *Journal of Physical Oceanography*, *52*(6), 1073–1089.

Meredith, M. P., & Hogg, A. M. (2006). Circumpolar response of southern ocean eddy activity to a change in the southern annular mode. *Geophysical Research Letters*, *33*(16).

Meredith, M. P., Woodworth, P. L., Chereskin, T. K., Marshall, D. P., Allison, L. C., Bigg, G. R., ... others (2011). Sustained monitoring of the southern ocean at drake passage: Past achievements and future priorities. *Reviews of Geophysics*, *49*(4).

Meyer, A., Langlais, C., Constantinou, N., Legresy, N., McC. Hogg, A., Navid, C., & Bindoff, N. (2023). Southern ocean meander structure trends and implications for carbon and heat uptake under a changing climate. *personal communication*.

Mikaloff Fletcher, S. E., Gruber, N., Jacobson, A. R., Doney, S. C., Dutkiewicz, S., Gerber, M., ... others (2006). Inverse estimates of anthropogenic co2 uptake, transport, and storage by the ocean. *Global biogeochemical cycles*, *20*(2).

Moore, J. K., Abbott, M. R., & Richman, J. G. (1997). Variability in the location of the antarctic polar front (90–20 w) from satellite sea surface temperature data. *Journal of Geophysical Research: Oceans*, *102*(C13), 27825–27833.

Moore, J. K., Abbott, M. R., & Richman, J. G. (1999). Location and dynamics of the antarctic polar front from satellite sea surface temperature data. *Journal of Geophysical Research: Oceans*, *104*(C2), 3059–3073.

Morris, M., Stanton, B., & Neil, H. (2001). Subantarctic oceanography around new zealand: preliminary results from an ongoing survey. *New Zealand Journal of Marine and Freshwater Research*, *35*(3), 499–519.

Morrison, A. K., Frölicher, T. L., & Sarmiento, J. L. (2015). Upwelling in the southern ocean. *Physics Today*, *68*(1), 27.

Murphy, E. J., Johnston, N. M., Hofmann, E. E., Phillips, R. A., Jackson, J. A., Constable, A. J., ... others (2021). Global connectivity of southern ocean ecosystems. *Frontiers in Ecology and Evolution*, 454.

Nardelli, B. B. (2013). Vortex waves and vertical motion in a mesoscale cyclonic eddy. *Journal of Geophysical Research: Oceans*, *118*(10), 5609–5624.

Naveira Garabato, A. C., Ferrari, R., & Polzin, K. L. (2011). Eddy stirring in the southern ocean. *Journal of Geophysical Research: Oceans*, *116*(C9).

Neil, H. L., Carter, L., & Morris, M. Y. (2004). Thermal isolation of campbell plateau, new zealand, by the antarctic circumpolar current over the past 130 kyr. *Paleoceanography*, *19*(4).

Newton, C. W. (1959). *Synoptic comparisons of jet stream and gulf stream systems* (Tech. Rep.). Chicago, Illinois, United States: University of Illinois Chicago.

Olbers, D., Borowski, D., Völker, C., & WOeLFF, J.-O. (2004). The dynamical balance, transport and circulation of the antarctic circumpolar current. *Antarctic science*, *16*(4), 439–470.

Onogi, K., Tsutsui, J., Koide, H., Sakamoto, M., Kobayashi, S., Hatsushika, H., ... Taira, R. (2007). *Japanese 55-year reanalysis* [dataset]. National Center for Atmospheric Research and Japan Meteorological Agency. Retrieved from `https://jra.kishou.go.jp/JRA-55/index_en.html#link` doi: 10.2151/jmsj.85.369

Orsi, A. H., Whitworth III, T., & Nowlin Jr, W. D. (1995). On the meridional extent and fronts of the antarctic circumpolar current. *Deep Sea Research Part I: Oceanographic Research Papers*, *42*(5), 641–673.

Peng, Q., Xie, S.-P., Wang, D., Huang, R. X., Chen, G., Shu, Y., ... Liu, W. (2022). Surface warming–induced global acceleration of upper ocean currents. *Science Advances*, *8*(16), eabj8394.

Phillips, H., & Bindoff, N. (2014). On the nonequivalent barotropic structure of the antarctic circumpolar current: An observational perspective. *Journal of Geophysical Research: Oceans*, *119*(8), 5221–5243.

Qiu, B., & Chen, S. (2006). Decadal variability in the large-scale sea surface height field of the south pacific ocean: Observations and causes. *Journal of physical oceanography*, *36*(9), 1751–1762.

Rintoul, S., & Naveira Garabato, A. (2013). Dynamics of the southern ocean circulation. In *International geophysics* (Vol. 103, pp. 471–492). Elsevier.

Roach, C. J., Balwada, D., & Speer, K. (2016). Horizontal mixing in the southern ocean from argo float trajectories. *Journal of Geophysical Research: Oceans*, *121*(8), 5570–5586.

Roemmich, D., Gilson, J., Davis, R., Sutton, P., Wijffels, S., & Riser, S. (2007). Decadal spinup of the south pacific subtropical gyre. *Journal of Physical Oceanography*, *37*(2), 162–173.

Rosso, I., Hogg, A. M., Kiss, A. E., & Gayen, B. (2015). Topographic influence on submesoscale dynamics in the southern ocean. *Geophysical Research Letters*, *42*(4), 1139–1147.

Ryan, W., Carbotte, S., Coplan, J., O'Hara, S., Melkonian, A., Arko, R., ... others (2009). *Global multi-resolution topography (gmrt) synthesis data set* [dataset]. Global Multi-Resolution Topography Synthesis. Retrieved from `https://www.gmrt.org/services/gridserverinfo.php#!/services/getGMRTGrid` doi: 10.1594/IEDA.100001

Sabine, C. L., Feely, R. A., Gruber, N., Key, R. M., Lee, K., Bullister, J. L., ... others (2004). The oceanic sink for anthropogenic co2. *science*, *305*(5682), 367–371.

Saenko, O. A., Fyfe, J. C., & England, M. H. (2005). On the response of the oceanic wind-driven circulation to atmospheric co2 increase. *Climate dynamics*, *25*, 415–426.

Sallée, J.-B., Matear, R. J., Rintoul, S. R., & Lenton, A. (2012). Localized subduction of anthropogenic carbon dioxide in the southern hemisphere oceans. *Nature Geoscience*, *5*(8), 579–584.

Sarmiento, J. L., Gruber, N., Brzezinski, M., & Dunne, J. (2004). High-latitude controls of thermocline nutrients and low latitude biological productivity. *Nature*, *427*(6969), 56–60.

Shao, A. E., Gille, S. T., Mecking, S., & Thompson, L. (2015). Properties of the subantarctic front and polar front from the skewness of sea level anomaly. *Journal of Geophysical Research: Oceans*, *120*(7), 5179–5193.

Shi, J.-R., Talley, L. D., Xie, S.-P., Peng, Q., & Liu, W. (2021). Ocean warming and accelerating southern ocean zonal flow. *Nature Climate Change*, *11*(12), 1090–1097.

Sokolov, S., & Rintoul, S. R. (2002). Structure of southern ocean fronts at 140 e. *Journal of Marine Systems*, *37*(1-3), 151–184.

Sokolov, S., & Rintoul, S. R. (2007a). Multiple jets of the antarctic circumpolar current south of australia. *Journal of Physical Oceanography*, *37*(5), 1394–1412.

Sokolov, S., & Rintoul, S. R. (2007b). On the relationship between fronts of the antarctic circumpolar current and surface chlorophyll concentrations in the southern ocean. *Journal of Geophysical Research: Oceans*, *112*(C7).

Sokolov, S., & Rintoul, S. R. (2009). Circumpolar structure and distribution of the antarctic circumpolar current fronts: 2. variability and relationship to sea

surface height. *Journal of Geophysical Research: Oceans*, *114*(C11).

Straub, D. N. (1993). On the transport and angular momentum balance of channel models of the antarctic circumpolar current. *Journal of physical oceanography*, *23*(4), 776–782.

Taburet, G., Sanchez-Roman, A., Ballarotta, M., Pujol, M.-I., Legeais, J.-F., Fournier, F., ... Dibarboure, G. (2019). Duacs dt2018: 25 years of reprocessed sea level altimetry products. *Ocean Science*, *15*(5), 1207–1224.

Tamsitt, V., Drake, H. F., Morrison, A. K., Talley, L. D., Dufour, C. O., Gray, A. R., ... others (2017). Spiraling pathways of global deep waters to the surface of the southern ocean. *Nature communications*, *8*(1), 172.

Thomas, S. D., Jones, D. C., Faul, A., Mackie, E., & Pauthenet, E. (2021). Defining southern ocean fronts using unsupervised classification. *Ocean Science*, *17*(6), 1545–1562.

Thompson, A. F. (2010). Jet formation and evolution in baroclinic turbulence with simple topography. *Journal of Physical Oceanography*, *40*(2), 257–278.

Thompson, A. F., Haynes, P. H., Wilson, C., & Richards, K. J. (2010). Rapid southern ocean front transitions in an eddy-resolving ocean gcm. *Geophysical research letters*, *37*(23).

Thompson, A. F., & Naveira Garabato, A. C. (2014). Equilibration of the antarctic circumpolar current by standing meanders. *Journal of Physical Oceanography*, *44*(7), 1811–1828.

Thompson, A. F., & Sallée, J.-B. (2012). Jets and topography: Jet transitions and the impact on transport in the antarctic circumpolar current. *Journal of physical Oceanography*, *42*(6), 956–972.

Toggweiler, J., & Samuels, B. (1995). Effect of drake passage on the global thermohaline circulation. *Deep Sea Research Part I: Oceanographic Research Papers*, *42*(4), 477–500.

Viglione, G. A., & Thompson, A. F. (2016). Lagrangian pathways of upwelling in the southern ocean. *Journal of Geophysical Research: Oceans*, *121*(8), 6295–6309.

Williams, R. G., Wilson, C., & Hughes, C. W. (2007). Ocean and atmosphere storm tracks: The role of eddy vorticity forcing. *Journal of Physical Oceanography*, *37*(9), 2267–2289.

Witter, D. L., & Chelton, D. B. (1998). Eddy–mean flow interaction in zonal oceanic jet flow along zonal ridge topography. *Journal of physical oceanography*, *28*(10), 2019–2039.

Xu, X., Chassignet, E. P., Firing, Y. L., & Donohue, K. (2020). Antarctic circumpolar current transport through drake passage: what can we learn from comparing high-resolution model results to observations? *Journal of Geophysical Research: Oceans*, *125*(7), e2020JC016365.

Youngs, M. K., Thompson, A. F., Lazar, A., & Richards, K. J. (2017). Acc meanders, energy transfer, and mixed barotropic–baroclinic instability. *Journal of Physical Oceanography*, *47*(6), 1291–1305.

Zhang, X., Nikurashin, M., Peña-Molino, B., Rintoul, S. R., & Doddridge, E. (2023). A theory of standing meanders of the antarctic circumpolar current and their response to wind. *Journal of Physical Oceanography*, *53*(1), 235–251.

Zhang, Y., Chambers, D., & Liang, X. (2021). Regional trends in southern ocean eddy kinetic energy. *Journal of Geophysical Research: Oceans*, *126*(6), e2020JC016973.